SAE International™

Measurement of Gaseous and Particulate Emissions from Algae-Based Fatty Acid Methyl Esters

2010-01-1523
Published
05/05/2010

Bethany C. Fisher, Anthony J. Marchese, John Volckens, Taehyoung Lee and Jeffrey L. Collett
Colorado State Univ.

Copyright © 2010 SAE International

ABSTRACT

Studies have shown that the magnitude of pollutant emissions (e.g. NO_x and PM) from diesel engines operating on fatty acid methyl esters (i.e. FAME biodiesel) are related to the fatty acid composition of the triglycerides present in the bio feedstock. Specifically, NO_x emissions have been shown to increase with increasing levels of unsaturation in the hydrocarbon chain and decrease with increasing carbon chain length; and PM emissions have been shown to decrease with increasing carbon chain length. Little work has been done to date to characterize the pollutant emissions of algae-based FAME, which have far different fatty acid composition than FAME derived from typical vegetable or animal fat feedstocks. Accordingly, the goal of the present study was to characterize the performance and emissions from a diesel engine operating on FAME with fatty acid composition commensurate with that produced from several algal species currently under consideration for wide scale fuel production. Tests were performed on a 2.4 L, 56 HP John Deere 4024T, non-road diesel engine meeting USEPA Tier 2 emissions regulations. The engine was fitted with a unique, low-volume fuel injection system that enabled emissions tests to be conducted with very low volumes of specialty fuel sample. Tests were performed on 9 different fuel blends at 2 different engine loading conditions. Exhaust gas measurements were made using a 5-gas emissions analysis system that includes chemiluminescence measurement of NO, NO_2 and total NO_x, flame ionization detection of total hydrocarbons and non-dispersive infrared detection of CO and CO_2. An FTIR was used to measure additional hazardous air pollutants such as formaldehyde. Particulate matter was characterized on-line, using an Aerodyne Aerosol Mass Spectrometer (AMS), which is capable of direct measurement of both particle size (50 and 1000 nm) and chemical composition. Smaller PM size distributions (10 to 100 nm) were measured using a Scanning Mobility Particle Sizer. Total PM mass emissions and the ratio of elemental carbon to organic were measured using gravimetric sampling. Results showed that the emissions from the two simulated algal methyl ester formulations were similar to those measured from soy and canola methyl esters with the exception of NO_x emissions which were shown to decrease for the simulated algal methyl esters. The decreased NO_x emissions from the simulated algal methyl esters were accompanied by a decrease in premixed burn fraction.

INTRODUCTION

Biofuels are considered to be renewable because the carbon present in the vegetable oil or animal fat feedstocks originates from carbon dioxide already present in the atmosphere as compared to fossil fuels in which the carbon in the fuel is liberated from beneath the surface of the earth and released into the atmosphere. Biofuels also offer additional benefits such as reducing dependence on imported petroleum and reduced CO, HC, SO_x and PM emissions. However, if biofuels are to attain a significant penetration into the global energy portfolio, the following issues still need to be addressed:

1. *The production of many biofuels is excessively energy intensive*. For example, although estimates vary, most studies suggest that for every 1 unit of energy contained in corn ethanol, the equivalent of 0.8 units of fossil fuel energy input are required [1,2].

2. *Most of the biofuels in use today result in very poor yield of fuel energy per acre of crop.* For example, 1 acre of soybeans yields only 60 gallons of biodiesel per year [3].

3. *Most current biofuels utilize feedstocks that might be better used to contribute to the limited global food supply*. In the United States, soy biodiesel and corn ethanol represent the overwhelming majority of transportation biofuels in

widespread production. Both directly compete with the global food supply.

4. *Many biofuels have significantly lower energy content than petroleum based fuels*. Ethanol, for example, has a lower heating value (MJ/liter) that is only 66% that of gasoline, which results in fuel economy penalties that limit its consumer appeal even among those who own flex fuel vehicles [4].

5. *In some cases, the combustion of biofuels can result in increases in some pollutants*. Although biofuels generally result in decreases in pollutant formation, some studies have shown that ethanol produces increased formaldehyde and acetaldehyde emissions [5] and biodiesel often produces increased NO_x emissions [6], increased particle-bound organic carbon emissions [7] and decreased mean particle diameter [8], which may have adverse health effects [9].

Algae-derived biofuels have the potential to solve each of the above issues, resulting in a high-yield, efficiently produced, renewable fuel that does not compete with the global food supply [10,11]. Many microalgae strains have been identified that produce up to 70% of their dry weight in lipid oil, which suggests that they can be converted to biofuels via lower energy processes. Furthermore, current estimates suggest that it may be possible to produce 5,000 gallons of biofuel per acre of algae, compared to 60 gallons per acre for soy biodiesel. Moreover, with hundreds of algal strains currently under consideration for full-scale production of algal bio-crude, the potential exists to select strains that minimize pollutant emissions, including NO_x and PM.

Algal bio-crude oil can be utilized as a liquid transportation fuel in a variety of forms including direct combustion of algal triglycerides (i.e. straight algal oil); conversion of the triglycerides into algal methyl esters (AME) or algal ethyl esters (AEE) via transesterification with methanol or ethanol; conversion into algal renewable diesel (ARD) for ground transportation or algal synthetic paraffinic kerosene (ASPK) as a blendstock for jet fuel. In addition, it is also possible to convert post-oil-extracted algal biomass into alcohols such as ethanol, n-butanol or n-pentanol. Because of the differences in complexity, cost and capital requirements and the variety of potential applications (compression ignition engines, spark ignition engines, aircraft engines, rail, marine, etc.) each of these forms of algae derived fuels are expected to obtain a niche in the future global transportation energy sector. Accordingly, it is anticipated that algal bio-crude will be converted into each of these forms of fuels in the years to come.

As detailed in the National Algal Biofuels Technology Roadmap [11], it is recognized that for any of the above algae-derived biofuels to obtain widespread penetration, they must qualify as "fit-for-purpose". A fuel is said to be fit-for-purpose if it meets regulatory and customer requirements when delivered to the refueling location. For AME and AEE, the anticipated end-use issues that must be addressed include lower oxidative and biological stability than petroleum diesel, the potential for higher NO_x emissions [6], uncertainty in the health effects associated with particulate emissions [8], and cold-weather performance problems. Additional issues include contamination of the esters with chlorophyll, metals, toxins, or catalyst poisons (e.g., sulfur, phosphorus) from the algal biomass and/or growth medium, undesired performance effects due to different algal fatty acid compositions and end-product variability. For ARD, the oxidative-stability problems are not expected to be as severe as that of AME/AEE and studies suggest that renewable diesel results in decreased NO_x emissions [12]. Given these concerns, the following primary research efforts were identified in the National Algal Biofuels Technology Roadmap [11] as required to enable optimal algae-derived fuel utilization:

- characterization studies to quantify contaminants and end-product variability depending on the production process;
- engine performance and emissions testing for early identification of undesired characteristics;
- tailoring the algal fatty-acid profile to mitigate fit-for-purpose issues and to ultimately enhance value relative to corresponding petroleum products.

The goal of the present study was to characterize the performance and emissions from a diesel engine operating on FAME with fatty acid composition commensurate with that produced from several algal species currently under consideration for wide scale fuel production.

FATTY ACID COMPOSITION OF ALGAL METHYL ESTERS

Like many other vegetable oil or animal fat feedstocks, algal bio-crude can be readily converted into biodiesel FAME via a simple transesterification process as shown in Fig. 1(a). After transesterification, the chemical constituents of biodiesel FAME consist of mixtures of saturated and unsaturated oxygenated mono-alkyl esters [13] containing carbon chains (i.e. R_1, R_2, and R_3 in Figure 1) of 10 to 24 atoms in length such as those shown in Fig. 1(b). As shown in Table 1, the length and degree of unsaturation of the carbon chains are highly dependent on the feedstock. For example, soybean FAME, which is currently the most common form of biodiesel produced in the United States, consists of approximately 14% saturated, 24% mono-unsaturated and 62% polyunsaturated methyl esters with an average carbon chain length of 18 [14]. Coconut FAME, on the other hand, consists of 93% fully saturated methyl esters with an average carbon chain length of only 12. Many algae strains currently under consideration for future production of FAME contain up to 30% highly unsaturated fatty acids that have five or more double bonds. The carbon chain length and degree of

unsaturation have been shown to have a profound impact on the NO_X and sooting characteristics of biodiesel [15,16]. For example, coconut FAME (which has shorter, saturated carbon chains) has been shown to produce significantly less NO_X but more soot than soybean FAME (which has longer, unsaturated carbon chains) [17].

(See Figure 1 after last section of paper.)

(See Table 1 after last section of paper.)

Table 1 also includes the fatty acid composition for two algal oils: *Nannochloropsis Oculata and Isochrysis Galbana 3*. The former algae species is currently under consideration for wide scale production and its fatty acid composition was measured from algal oil samples provided by Solix Biofuels [18]. The fatty acid composition for the latter species was obtained from the literature [19] where the 3 indicates that the oil was produced in the late stationary phase of growth. As shown in Table 1, the fatty acid composition from these algal oils differ from the traditional vegetable oil feedstocks in that they contain substantial quantities of eicosapentaenoic acid (EPA, C20:5) and docosahexaenoic acid (DHA, C22:6) which are omega-3 acids containing 5 and 6 double bonds, respectively. Indeed, a large body of data exists on the fatty acids derived from these algae species as a source of omega-3 acids for human nutritional supplements [20,21]. However, little or no data exist on the combustion and pollutant formation mechanisms of highly unsaturated esters such as eicosapentaeonic acid methyl ester. Moreover, it is well documented that the fatty acid composition varies widely among microalgae species [22] and is also influenced by the physical conditions under which the algae is cultivated, including light intensity [23], temperature [24], pH [25], salinity [26] and the stage of growth during which the algae is harvested [19].

EFFECT OF FATTY ACID CHEMICAL STRUCTURE ON POLLUTANT FORMATION

Studies have shown that the magnitude of pollutant emissions (e.g. NO_X and PM) from diesel engines operating on fatty acid methyl esters (i.e. FAME biodiesel) are directly linked to the chemical structure of the triglycerides present in the bio feedstock. Specifically, NO_X emissions have been shown to increase with increasing number of double bonds in the hydrocarbon chain and decrease with increasing carbon chain length; and PM emissions have been shown to decrease with increasing carbon chain length [15,16]. However, no study has been done to date to characterize the pollutant emissions of algae-derived FAME, which have far different fatty acid composition than FAME derived from typical vegetable or animal fat feedstocks. Accordingly, the goal of the present study is to examine the effect of the chemical structure of algal bio-crude feedstocks on pollutant formation in a diesel engine operating on algae-derived FAME biodiesel.

McCormick and coworkers [15] were the first to investigate the effects of fatty acid chain length and degree of unsaturation on PM and NO_X emissions. For neat fully saturated methyl esters, they found that NO_X emissions decreased and PM emissions increased with increasing chain length. For a fixed carbon chain length of 18, they found that brake specific NO_X emissions increased linearly with the number of double bonds from 4.2 g/BHP-hr for C18:0 to 5.6 g/BHP-hr for C18:3. In terms of PM, they found that C18:2 produced much higher brake specific PM emissions than any of the other C18 methyl esters.

A similar study, conducted by Schonborn and coworkers [16], used an ultra low volume fuel injection system with a single cylinder diesel engine to test small quantities of pure fatty acid alkyl esters. To examine the effect of chain length, they performed tests with saturated methyl esters C12:0 through C22:0 and found that NO_X decreased with increasing chain length, with the C22:0 producing 20% less NO_X than petroleum diesel. Total PM mass emissions, on the other hand, were low and relatively constant between the four shorter saturated methyl esters but much higher for C22:0. To examine the effect of double bonds, C18:0, C18:1 and C18:2 methyl esters were studied. In agreement with the earlier study of McCormick and coworkers [15], NOx emissions were found to increase with increasing number of double bonds with C18:2 producing 40% more NO_X than petroleum diesel. In the Schonborn [16] study, total PM mass emissions also increased as the degree of saturation increased. Specifically, both C18:0 and C18:1 produced less PM than petroleum diesel, whereas C18:2 emitted about 25% more mass than diesel.

As shown in Table 1, algal methyl esters differ from typical feedstocks in that they may contain high levels of highly unsaturated fatty acids EPA(C20:5) and DHA (C22:6). Based on the results of these previous studies [15,16], prior to the present work it was unclear how the presence of EPA and DHA would affect PM and NO_X emissions since increased chain length and increased double bonds have opposite effects on the emissions of these pollutants. However, both studies suggest that the number of double bonds has a greater effect on NO_X production than chain length. Therefore, prior to the present work, an increase in NO_X was expected for the algal methyl esters.

Although NO_X and particulate matter were the focus of the two aforementioned studies, it is also possible that combustion of algal methyl esters might produce anomalous amounts of other pollutants. As mentioned above, the oil produced by algae is different from all types of oil currently

used to produce biodiesel and no emissions studies of algal methyl esters had been conducted prior to the present study. Accordingly, this work examines how the emissions of this new fuel source might compare against emissions from both petroleum diesel and more traditional biodiesel such as soy methyl esters and canola (rapeseed) methyl esters.

EXPERIMENTAL PROCEDURE

To determine the effect of the algal oil composition on engine emissions, two different algae-based oils with different amounts of EPA and DHA were transesterified to biodiesel FAME and their emissions were compared against that of soy biodiesel, rapeseed biodiesel, petroleum diesel and blends thereof. Emissions testing was performed using a John Deere 4024T, non-road diesel engine meeting USEPA Tier 2 emissions regulations as described below.

ENGINE/ DYNAMOMETER DESCRIPTION

The test engine was a four-cylinder, turbocharged, water cooled, off-road John Deere model 4024T built in 2003. The total displacement of the engine was 2.4 L with a rated power of 39 kW at 2400 rpm. Mechanically controlled unit injector pumps delivered fuel to the cylinders and the injection timing was unaltered for the tests presented herein. The load on the engine was applied by a water-cooled eddy current or induction dynamometer, made by Mid-West Dynamometers. The speed of the engine, the load produced by the dynamometer, and the resulting power were all measured by the dynamometer control unit. The speed of the engine was set using a voltage-controlled throttle, while the load was set independently by the dynamometer control unit. The engine speed was measured with a Hall Effect RPM sensor.

Two Micro Motion CMF010 Coriolis mass flow meters were used to measure the mass flow rate of the specialty and petroleum based fuels, respectively. Eleven type K thermocouples were used to monitor temperature in the fuel system as well as other engine operating parameters, such as oil temperature and exhaust temperature. The boost pressure produced by the turbocharger was measured with an Omega PX181B-030G5V pressure transducer. Data were acquired using a National Instruments Compact RIO (cRIO) 9074 data acquisition/control system, which was controlled and monitored using LabVIEW. High-speed Kistler 6056A pressure transducers were installed in two of the engine glow plug adapters to measure the in-cylinder pressure in two of the four cylinders. The data from these high speed pressure transducers were collected by a Hi-Techniques Win600 computer.

TEST MATRIX

For this study, the 4024T John Deere engine was operated at rated speed (2400 RPM) at two different loads (80 N-m and 115 N-m), which correspond to 50% and 75% of the maximum torque at rated speed. Nine different fuel formulations were tested and each load/fuel test point was repeated twice:

- Ultra low sulfur diesel (ULSD),
- Soy methyl ester biodiesel (Soy B100),
- 20% soy methyl ester/80% ULSD (Soy B20),
- Canola methyl ester biodiesel (Canola B100),
- 20% canola methyl ester/80% ULSD (Canola B20),
- Algal methyl ester #1 (Algae 1 B100),
- 20% algal methyl ester #1/ 80% ULSD (Algae 1 B20),
- Algal methyl ester #2 (Algae 2 B100), and
- 20% algal methyl ester #1/ 80% ULSD (Algae 2 B20).

As described in the following section, algal methyl ester 1 and 2 were formulated to match the fatty acid compositions of *Nannochloropsis Oculata* and *Isochrysis Galbana 3*, respectively. The former algae species was chose because it is currently under consideration for wide scale fuel production [1,18] and it contains approximately 20% highly unsaturated fatty acids. The latter algae species was chosen as the second algal oil because it contains roughly 10% highly unsaturated fatty acids, which is approximately half the amount of highly unsaturated fatty acids found in the *Nannochloropsis Oculata* fatty acid profile.

ALGAE-BASED METHYL ESTER FORMULATION

Numerous start-up companies are competing globally to develop proprietary systems and processes for maximizing algae growth for the production of biofuels [18]. However, no such companies are currently at full scale production and algal oil is currently a scarce commodity. Therefore, it was cost prohibitive to obtain algal fuel samples large enough to accommodate the necessary emissions test matrix. Accordingly, “composite” algal methyl ester formulations were produced by transesterifying pharmaceutical grade fish oil and mixing it with a variety of pure methyl esters. Using this technique, two different synthetic algal-based FAME fuels were produced. The first fuel had approximately 20% by volume omega-3 fatty acids (with >4 double bonds) and the second fuel contained approximately 10% omega-3 fatty acids.

Pharmaceutical grade fish oil from Jedwards International was transesterified in small batches to ensure that the oil was fully reacted and properly washed. Palmitic acid methyl ester (C16:0) and Oleic acid methyl ester (C18:1) were obtained from Procter & Gamble Chemical Division and added to the transesterified fish oil biodiesel in two different ratios to simulate *Nannochloropsis Oculata* and *Isochrysis Galbana 3*, respectively. Table 2 shows that the fatty acid composition of the composite algal methyl esters compared favorably with that *Nannochloropsis Oculata* and *Isochrysis Galbana 3* based on the total amount of double bonds. The previous work of Grabowski et al. [15] and Schonborn et al. [16] indicates that the number of double bonds in the fatty acid has a greater effect on emissions than chain length, so the profiles were matched based on the number of double bonds.

(See Table 2 after last section of paper.)

Table 3 contains the results of fuel analysis that was performed to characterize the properties of the ULSD and the four B100 methyl ester formulations. As expected, the methyl ester formulations all had higher density, higher bulk modulus, decreased lower heating value and increased cloud point. The lower heating value for the algal methyl ester formulations was nearly identical to that of the soy and canola methyl esters.

(See Table 3 after last section of paper.)

LOW VOLUME FUEL INJECTION SYSTEM

To accommodate low volumes of specialty fuels such as those described above, the John Deere 4024T engine was modified to isolate the fuel system for one of the four cylinders. This system enabled a single cylinder to operate on one fuel, while the remaining cylinders ran on petroleum diesel at all times. The stock engine configuration employs a single fuel intake line that feeds into a fuel galley that supplies fuel to each of the four cylinders. A fuel return line collects all the excess fuel from each cylinder and sends the return fuel out of the engine block. To isolate one of the four cylinders, a long hollow bolt was inserted into a threaded hole that extended to the inlet of the unit pump. This bolt blocked fuel from the common fuel galley from being fed into the unit pump and also provided a means to supply a different fuel to that cylinder. The end of the bolt on the outside of the engine was then mated to stainless steel Swagelok fuel lines. An identical bolt was used on the return side of the pump to collect any excess fuel. All four cylinders were operated on petroleum diesel during warm up, cool down, and after each test to ensure consistency between tests. A remotely controlled three-way valve regulated the fuel source for cylinder 4 between the main diesel tank and a separate, smaller tank containing the fuel of interest. The fuel delivery system is shown schematically in Figure 2. The 4024T engine and completed fuel delivery system is shown photographically in Figure 3.

(See Figure 2 after last section of paper.)

(See Figure 3 after last section of paper.)

EXHAUST SAMPLING

To measure the emissions from the isolated cylinder running on the fuel of interest, emissions probes were located directly in the exhaust manifold upstream of the location where the exhaust mixed with the gases from the other three cylinders. The gaseous probe and the particulate probe were sized and oriented according to 40 CFR Part 60 and ISO 8178 standards, but all the requirements in these standards could not be met because of geometrical constraints of the exhaust manifold. The aforementioned standards require that the probes be inserted eight diameters downstream and two diameters upstream from any disturbance such as a bend or contraction in a straight pipe. However, since all measurements were taken with the same experimental setup and test protocol, results for the different fuels should be consistent. Moreover, the brake specific emissions of all criteria pollutants reported herein were consistent with previous studies conducted using the same engine [8,27]. The orientation of the exhaust probes in the exhaust manifold is presented in Figure 4. Four sample probes were installed on exhaust port for cylinder 4, the isolated cylinder, while two probes were used to monitor cylinder 1, the other outer cylinder, for direct comparison against cylinder 4. As shown in Figure 4, a probe for all the gaseous measurements, a probe for all the particulate measurements, a thermocouple and a probe for the Cambustion CLD500 Fast NO_x analyzer were clustered around the exhaust port for cylinder 4. Another Fast NO_x probe and thermocouple port were located at the exhaust port for cylinder 1. Since cylinder 1 was always operated on petroleum diesel, the temperature and NO_x concentration in this cylinder provided a real-time comparison to the specialty fuel exhaust gases from cylinder 4. Heated sample lines carried the exhaust gases from the particulate probe to a dilution tunnel and from the gaseous probe to the 5-gas analyzer and Fourier Transform Infrared spectrometer. The sample lines were heated to 110 °C for the gaseous line and to 150 °C for the particulate line to prevent condensation in the exhaust.

(See Figure 4 after last section of paper.)

EXHAUST MEASUREMENTS

A total of seven instruments were used to characterize the gaseous and particulate components of the engine exhaust. Exhaust gas measurements were made using a 5-gas emissions analysis system that includes chemiluminescence measurement of NO, NO_2 and total NO_x, flame ionization

detection of total hydrocarbons and non-dispersive infrared detection of CO and CO_2. A Nicolet Magna-560 Fourier Transform Infrared Spectrometer (FTIR) was used to measure additional hazardous air pollutants such as formaldehyde. A Cambustion CLD500 Fast NO_x analyzer also measured NO. Total PM mass emissions were measured gravimetrically via collection on to Teflon filters, and elemental and organic carbon were measured via collection on (and subsequent analysis of) quartz filters. A Grimm Technologies Sequential Mobility Particle Sizer (SMPS) was used to measure particle size distributions from 10 to 1000nm. An Aerodyne High-Resolution Time-of-Flight Aerosol Mass Spectrometer (AMS) was used to analyze the chemical composition of the organic carbon particles. Kistler 6056A high speed pressure transducers recorded the in-cylinder pressure of cylinders 1 and 4. Detailed descriptions of all instrumentation and the associated test protocol for all gaseous and particulate measurement techniques are provided in [28].

All of the PM measurements were taken after the exhaust sample was diluted with clean air in a dilution tunnel. A 150 °C heated sample line delivered the exhaust sample to the dilution tunnel to prevent the gases from condensing while en route. A Venturi flow meter (also heated to 150°C) was used to measure the flow rate of the exhaust air sample entering the dilution tunnel. The dilution air was first cleaned by a HEPA filter, followed by an activated charcoal filter. A turbine flow meter was used to measure the flow rate of clean dilution air. A valve located downstream of the turbine flow meter was used to control the dilution ratio, which was maintained at 40:1 for all of the tests reported herein [28].

EXPERIMENTAL RESULTS

The brake power produced by the isolated cylinder is an important quantity for data analysis, but the traditional method of using the power measured by the dynamometer could not be used since all four cylinders were not always operating on the same fuel. Accordingly, the in-cylinder pressure transducers were used to calculate indicated power, which is defined as the net PdV power produced by combustion of the fuel-air mixture in the cylinder. Two Kistler 6056A in-cylinder pressure transducers were installed in the two outer cylinders so that the indicated power could be measured for the cylinder operating on the specialty fuel and one of the cylinders that always operated on ULSD. Using these two values along with the total brake power for the whole engine as measured by the dynamometer, it was possible to determine the percentage of the total brake power attributed to the specialty fuel cylinder 4. This technique relies on the assumption that the mechanical efficiency of the engine is independent of fuel type.

BRAKE SPECIFIC FUEL CONSUMPTION

Figure 5 contains the results of brake specific fuel consumption (BSFC) in g/bkWh for each of the nine fuels tested at both loading conditions. The error bars represent the observed experimental variation for the two tests performed for each fuel/engine load condition. For all of the results reported herein the observed variation was within the experimental uncertainty based on a detailed uncertainty analysis [28]. The results in Fig. 5 show that the BSFC was higher for all of the FAME biodiesel blends in comparison to ULSD. The results also show that the B100 FAME fuels exhibited higher brake specific fuel consumption than the B20 blends. The two algal methyl ester formulations exhibited comparable BSFC to that of the soy and canola methyl esters.

(See Figure 5 after last section of paper.)

The BSFC for all of the B100 blends was 10-12% higher than ULSD, with Algae 2 B100 consuming slightly more than the other methyl esters. Previous studies have reported BSFC increases of approximately 10% for B100 fuels, which is consistent with these results [29].

Also it should be noted that since fuels are purchased by volume, it is also relevant from a consumer standpoint to examine the volumetric brake specific volumetric fuel consumption. For example, the density of ULSD is 830 kg/m^3 and the density of canola methyl ester is 880 kg/m^3. At 50% load, the BSFC for Canola B100 is 326 g/bkWh compared to 292 g/bkWh for ULSD, which represents an increase of 12%. On a volume basis, the Canola B100 had a brake specific fuel consumption of 0.370 L/bkWh compared to 0.352 L/bkWh for ULSD at the same conditions, which represents an increase of only 5%.

The increase in BSFC for the FAME fuels is due to their lower energy content. The average lower heating value for the FAME fuels tested herein is approximately 13% lower than that of ULSD. The thermal efficiency takes into account the brake specific fuel consumption and the lower heating value for the fuel. As shown in Fig. 6, based on the overall thermal efficiency, the engine actually operated more efficiently on the B100 fuels at both loading conditions as evidenced from the slight increase in overall efficiency.

(See Figure 6 after last section of paper.)

GASEOUS EMISSIONS

For each test point, a five minute data set for the 5-gas analyzer and FTIR was collected during steady state operation. The raw gaseous mole fraction data were averaged over the five minute duration. Since a variety of different

fuels and different engine loads were employed during this test, a more relevant way to present gaseous emissions data is in terms of brake specific emissions (g/bkWh). A carbon balance between the carbon burned in the fuel and the carbon emitted as carbon monoxide, carbon dioxide, and total hydrocarbons was used to calculate the brake specific emissions. This analysis assumes that all the carbon in the exhaust comes from the carbon in the fuel. Equation (1) was used to find the brake specific emissions for gaseous species i:

$$BSE_i = \frac{\dot{m}_f \cdot \alpha_f \cdot Y_i \cdot MW_i}{\dot{W}_b \cdot MW_f \cdot \sum_{exhaust} Y_j \alpha_j} \quad (1)$$

where $\dot{m}_f$ is the mass flow rate of fuel to the isolate cylinder, α_f the average number of carbon molecules in the fuel, Y_i the fraction of ith species in the exhaust, MW_i the molecular weight of ith species, $\dot{W}_b$ the brake power generated by the single cylinder, MW_f the molecular weight of the fuel, and $\sum_{exhaust} Y_j \alpha_j$ the sum of the number of carbon molecules found in the exhaust constituents. This calculation accounts for differences in fuel composition and power produced. This formula was used for both the 5-Gas data and the FTIR data.

Gaseous Criteria Pollutant Emissions

Figures 7,8,9 show the brake specific emissions for carbon monoxide (CO), total hydrocarbons (THC), and oxides of nitrogen (NO_x) for all 9 fuels at 50% and 75% load, respectively. The error bars represent the range of the two runs for each data point. As discussed above, most studies have shown that CO and THC decrease but NO_x increases when operating a diesel engine on B100 FAME in comparison to petroleum diesel [6]. This result is also typically found for blends of FAME with petroleum diesel, although it has been found that the results are highly dependent on the engine type, engine duty cycle and biodiesel feedstock [30]. Emissions of NO_x tend to increase with increasing levels of unsaturation in the methyl ester hydrocarbon chain [15,16]. Due to the long and highly unsaturated fatty acid methyl ester content in the two algal methyl ester formulations, it was anticipated that that these fuels might produce even more NO_x than is generally seen with biodiesel.

(See Figure 7 after last section of paper.)

As shown in Fig. 7, the CO produced by the all of the biodiesel blends was less than that produced by ULSD at the lower load, with the B100 fuels producing less CO than the B20 fuels. These results are consistent with previous studies [6]. At the higher load, however, only the soy biodiesel blends reduced the carbon monoxide emitted relative to ULSD. However, it should be noted that the level of CO emissions at both loads is well below the current emissions regulations for this size and type of engine. Specifically, for an off-road Tier 2 engine producing a maximum of 39 kW, the 2007 standards limit CO to 5.0 g/kWh [31]. All of the fuels at both loads meet this standard. Figure 7 shows that the algal methyl ester formulations tested herein resulted in CO emissions similar to those of soy and canola methyl esters.

(See Figure 8 after last section of paper.)

As shown in Fig. 8, all of the B100 FAME blends resulted in a reduction in THC in comparison to ULSD at both loads. The B20 blends emitted higher levels of THC, with Algae 1 B20 producing the highest level for both loads. It should be noted that, for this class of engine, total hydrocarbons alone are not regulated. Rather, current EPA standards call for the regulation of the sum of NO_x and non-methane hydrocarbons (NMHC). For fuels like diesel and biodiesel, very little of the hydrocarbons emitted will be methane. The FTIR is set up to measure methane but the levels of methane detected were small in comparison to the total hydrocarbon measurement and the uncertainty in the methane measurement was larger than the measured concentration, making it statistically insignificant. Therefore, total hydrocarbons measured by the 5-Gas analyzer can be considered equivalent to non-methane hydrocarbons. The current NO_x+NMHC regulation for this size of engine is 4.7 g/bkWh, with the majority of that total coming from NO_x.

(See Figure 9 after last section of paper.)

Figure 9 shows that, contrary to expectations based on earlier research, the NO_x emissions produced by the two algal methyl ester formulations did not increase relative to the other FAME fuels or ULSD. Rather, both of the algal methyl ester formulations produced a reduction in NO_x emissions of approximately 10% and 2% at 50 % and 75 % load, respectively. In fact, the only B100 methyl esters to reduce NO_x at both loads were Algae 1 and Algae 2. At the higher load, the Soy B100 and Canola B100 produced an increase in NO_x emissions of 6% and 4% compared to ULSD, which is consistent with previous studies [15,16]. Also, the soy methyl esters consistently produced higher NO_x emissions that the canola methyl esters for all of the loading conditions and blending levels tested herein. These results are also consistent with previous studies [15,16].

Relationship Between Premixed Burn Fraction and NO_x Emissions

The in-cylinder pressure transducer records high speed pressure data, which can be plotted as a function of crank angle. The known geometry of the cylinder and connecting rod can then be used to calculate the cylinder volume as a function of crank angle. Pressure versus volume curves can

then be used to calculate the apparent rate of heat release (J/deg) due to fuel combustion in the cylinder. The apparent heat release rate calculation assumes a rate of heat loss to the cylinder walls and some additional losses due to crevice effects. As detailed in [28] a LabVIEW program was used to convert pressure vs. crank angle to apparent heat release rate given the engine geometry. The apparent heat release rate curves (J/deg) are presented in Figs. 10 and 11 for the B20 methyl ester blends at 50% and 75% load, respectively. For brevity, only the B20 blend heat release results are included herein. The B100 methyl ester results are detailed elsewhere [28].

(See Figure 10 after last section of paper.)

(See Figure 11 after last section of paper.)

There are several phenomena to note in Figs. 10 and 11. Firstly, all of the methyl esters resulted in an advance in the start of combustion in comparison to the ULSD. This result is not unexpected since, for engines equipped with mechanical fuel injection systems, many studies have reported that methyl esters result in an advance in the start of injection (and thereby the start of combustion) because of the higher bulk modulus (a measure of the speed of sound in a liquid) of methyl esters with respect to petroleum diesel [32]. The advance in the start of injection effect is expected to be more pronounced in engines equipped with pump-line-nozzle injection systems (such as that employed in Ref. 32) than those equipped with mechanical unit injectors (such as that employed herein) because the former systems have longer lengths of high pressure injection lines. However, the John Deere 4024T fuel injection system includes a length of approximately 4 inches of high pressure line between each pumping unit and its respective nozzle assembly. Accordingly, it is highly possible that this configuration would yield a slight advance in start of injection for methyl esters and studies have shown that even minute injection timing shifts can contribute to changes in NO_X emissions because of the very strong dependence of combustion phasing on NO_X formation.

For the present study, the fuel injectors of the 4024T engine were not instrumented, so there was no way to distinguish between an advance in start of combustion due to advance in injection timing or a decrease in the ignition delay. Accordingly, the advance in start of combustion could be a combination of both effects. The advance in start of combustion is more pronounced with B100 blends, with Canola B100, Algae 1 B100 and Algae 2 B100 starting combustion even a few degrees before Soy B100.

The second characteristic of note in Figs. 10 and 11 is the height of (and integrated area underneath) the initial peak in the heat release rate curve, which indicates the rate of heat release during the premixed combustion phase. As shown in Fig. 10 and 11, for example, the height of the premixed combustion peak for Soy B20 is approximately the same as ULSD, but advanced by a few degrees. However, for all of the other B20 methyl esters, the height of the premixed combustion peaks are much lower than that of ULSD. Similar results were observed for B100 blends.

Numerous mechanisms have been hypothesized for the increased NO_X emissions often observed for methyl esters including effects related to differences in viscosity [33], bulk modulus [34], boiling point [35], adiabatic flame temperature [36], radiative heat loss [37] and their effects on thermal NO_X and/or prompt NO_X production. A recent optical engine study [38] has strongly suggested that biodiesel NO_X increases are a consequence of increased fraction of the heat release occurring in the premixed autoignition zone. The mechanism by which increased premixed burn fraction produces increased NO_X emissions has yet to be explained but theories include higher local and average in-cylinder temperature, less radiative heat loss, higher O-atom concentrations and/or increased prompt NO_X production.

Although many competing mechanisms may be involved, it is apparent that methyl ester NO_X increases are related to premixed combustion phenomena. One way to quantify the amount of fuel burned in the premixed phase is to examine the ratio of the heat release generated in the premixed phase relative to all the heat released in the cycle. This ratio is called the premixed burn fraction. The premixed burn fraction was determined by dividing the integrated area below the initial peak in the heat release rate curve by the area under the entire curve. Figure 12, which is a plot of brake specific NO_X emissions versus premixed burn fraction, clearly demonstrates a relationship between premixed burn fraction and NO_X emission for all of the fuel/load conditions considered in this study. The data points are colored to indicate the fuel type and the load is identified by the data point shape: diamond-shaped points represent 50% load and circles denote 75% load. The data shows that, for the experiments presented here, the NO_X emissions varied linearly with premixed burn fraction.

(See Figure 12 after last section of paper.)

ALDEHYDE EMISSIONS

In addition to the 5-Gas analyzer, a Nicolet Magna 560 FTIR was used to measure a variety of gaseous species including oxides of nitrogen, oxides of sulfur and various hydrocarbon species that are considered hazardous air pollutants, such as aldehydes. Two exhaust species of interest that were measured in significant quantities in the FTIR data were formaldehyde and acetaldehyde. The brake specific emissions for these two aldehydes are shown below in Figures 13 and

14, with the error bars representing the range of the two sets of data taken.

(See Figure 13 after last section of paper.)

In contrast to the brake specific CO and THC emissions results presented above, which showed little difference between the emissions observed for the algal methyl esters in comparison to the more traditional soy and canola methyl esters, Fig. 13 shows that the algal methyl esters consistently produced higher formaldehyde emissions than either soy or canola. Prior studies have not shown consistent results for aldehyde emissions from methyl esters. The majority of studies have shown that aldehyde emissions decrease with the use of methyl esters but some studies have reported the opposite effect [14,38]. Other studies have reported a decrease in formaldehyde emissions, but an increase in acetaldehyde emissions [39,40]. The soy and canola methyl ester blends tested in this study exhibited a decrease in formaldehyde in comparison with ULSD at both loads, which is consistent with the majority of previous tests that reported decreased formaldehyde emissions for these same fuels. Although formaldehyde is not currently a regulated emission for engines of this size, formaldehyde is classified as an air toxin by the EPA, so it could become a regulated compound in the future. Accordingly, the increased formaldehyde emissions observed in the study for both algal methyl ester formulations may require further study.

(See Figure 14 after last section of paper.)

Figure 14 contains a plot of brake specific acetaldehyde emissions for all fuels at both engine loading conditions. At the lower load, all B100 methyl esters produced nearly identical acetaldehyde emissions, which corresponded to an approximately 20% decrease with respect to ULSD. At the higher loading condition, Canola B100 and Algae 2 B100 produced slightly higher acetaldehyde emissions than the other methyl esters, but all of the methyl esters resulted in decreased acetaldehyde emissions relative to ULSD at the higher loading condition as well. At 50% load, the Algae 1 B20 and Algae 2 B20 blends resulted in slight increases in acetaldehyde emissions. Similar to formaldehyde, previous studies have not produced consistent results with respect to acetaldehyde emissions from methyl esters.

PARTICULATE MATTER MASS EMISSIONS

Figure 15 contains a plot of total brake specific PM mass emissions for all fuels at both engine loading conditions. Most studies show that total PM mass emissions decrease for methyl ester biodiesel in comparison to petroleum diesel [6]. With the exception of Algae 1 B100 at the low load condition, all of the B100 fuels produced substantial reductions total PM mass emissions at both load conditions. At the high load condition, reductions of up to 40% were observed for the methyl esters. The B20 blends resulted in little reduction in particulate mass and, in some cases, resulted in slight increases in PM mass emissions. The results suggest that algal methyl esters should not be a concern from a total PM mass emissions standpoint.

(See Figure 15 after last section of paper.)

PARTICULATE MATTER SIZE DISTRIBUTION

Figures 16 and 17 contain the PM size distribution as measured by the SMPS for the B100 methyl esters in comparison with ULSD for the 50% and 75% loading conditions, respectively. Results for B20 methyl ester blends are reported elsewhere [28]. The PM size distribution is measured as the number of particles per volume and then normalized by the logarithm of the bin widths. This normalization accounts for the variation in bin sizes used to count the particles. Mobility diameter is shown on a log scale on the x-axis since there is a wide range of sizes measured. The data shown in Figs. 16 and 17 represent averages of at least four data sets but error bars were omitted from the plots for clarity. The standard deviation on the curves is generally small, although the variation in the nucleation mode (the secondary peak observed at smaller diameters for some fuels) is much higher than in the rest of the data [28]. As an example, Figure 18 contains a PM size distribution plot containing standard deviation error bars for Soy B100 at 50% and 75% load, respectively. Error bars for all the SMPS results were of the same order as those shown in Figure 19.

(See Figure 16 after last section of paper.)

(See Figure 17 after last section of paper.)

(See Figure 18 after last section of paper.)

Prior research, including studies performed at CSU using the same John Deere 4024T engine, have shown that soy methyl ester biodiesel produces particulates with a smaller mean mobility diameter than petroleum based diesel [7,27]. The results shown in Figs. 16 and 17 are consistent with these previous studies. In fact, all of the methyl ester formulations resulted in a reduction in mean particle mobility diameter as signified by the leftward shift in the mode of the distribution for the methyl ester fuels in comparison with the ULSD. The canola methyl ester blends produced the highest concentration of particles at all blends and loads whereas the soy methyl ester blends generated the lowest particle concentration in all cases. The two algal methyl esters produced particles with size distributions in between that of canola and soy methyl esters.

As shown in Figs. 16 and 17, several of the methyl ester fuels produced PM size distributions that exhibited a second peak in the 10 to 30 nm range, which corresponds to particles in the nucleation mode. Combustion generated particulates are comprised of many small particles that agglomerate to form larger complex particulates. The smaller nucleation particles are generally comprised of liquid volatile organic compounds and sulfuric acid, as opposed to the larger particles found in the accumulation mode that are made up of agglomerated carbon particles [41,42]. The formation mechanism for the nucleation mode particles is not well understood. Some studies have shown that the sulfur content in the fuel is responsible for the formation of nucleation mode particles and other studies have shown that both low and high sulfur fuels can produce these particles, depending on the engine load [43]. Since methyl esters contain little or no sulfur, it is unlikely that sulfur was responsible for the nucleation mode particles produced by the B100 methyl esters tested in this study.

Figures 16 and 17 show that at 50% load, the canola, soy and algae 1 methyl esters all exhibited a substantial nucleation mode peak, while at 75% load only the canola fuel exhibited the nucleation mode peak. These results suggest an area of future research as it is difficult to draw any conclusions as to why some of the methyl esters exhibited the large nucleation mode peaks and others did not. Impurities from the transesterification process are a consideration that should be mentioned since the canola methyl esters and algal methyl esters were produced in-house. However, at 50% load, the soy methyl esters, which were produced commercially, also exhibited the nucleation mode peak. Moreover, the algal methyl esters were produced at the bench scale, while the canola methyl esters were produced in a 20-gallon batch reactor [28]. Therefore, since three separate transesterification systems all produced fuels that exhibited the nucleation mode peak it is not believed that the nucleation mode peaks are an artifact from impurities from a particular transesterification process. Some studies have concluded that the formation of nucleation mode particles is highly dependent on exhaust temperature, humidity and dilution ratio [42]. Therefore, it is also possible that slight differences in the sampling environment between the various experiments are responsible for the formation of the nucleation mode particles.

ELEMENTAL CARBON (EC) AND ORGANIC CARBON (OC) ANALYSIS

The quartz filters used to capture the particulate matter were analyzed for their elemental and organic carbon content using a Sunset Labs OC/EC Analyzer as detailed in [28]. A single, 2.27 cm^2 punch was analyzed from each quartz filter. To correct for a positive artifact from possible adsorption of gaseous organic carbon, the organic carbon found on the main quartz filter was corrected by the use of a second quartz filter, which was located behind the Teflon filter used for the total PM mass emissions measurements. This second quartz filter collected only the gaseous organic carbon that could bias the particulate organic carbon measurement. For each test point, the organic carbon found on the second filter was subtracted from the organic carbon measurement from the front filter, resulting in a corrected organic carbon measurement.

Using the average elemental carbon mass and average corrected organic carbon mass, the brake specific EC and OC were calculated using a similar technique to that employed for the total brake specific PM emissions. Figures 19 and 20 show the brake specific EC and brake specific OC mass emissions for each fuel at 50 % and 75 % engine load, respectively. The error bars in the figures represent the range of the data between the two tests conducted at each operating condition. For both loads, all of the B100 methyl esters resulted in decreased EC in comparison to ULSD. At 50% load, the mass emissions of OC increased substantially for all of the B100 methyl esters in comparison to that measured for the ULSD. At 75% load, however, the mass emissions of OC for the B100 methyl esters were similar to that measured for ULSD. For the B20 methyl ester blends, the mass emissions of EC were similar to that measured for the ULSD, whereas the mass emissions of OC were higher for the B20 methyl esters in comparison to ULSD. These results are consistent with previous studies that have reported decreases in mass emissions of EC and increases in mass emissions of OC for methyl esters in comparison with petroleum diesel [7,27,44]. In general, the algal methyl esters produced slightly higher levels of OC in comparison to the soy and canola methyl esters with Algae 1 B100 at 50% engine load producing the highest mass emissions of OC among all of the fuel/engine load conditions tested in this study.

(See Figure 19 after last section of paper.)

(See Figure 20 after last section of paper.)

AEROSOL MASS SPECTROMETER RESULTS

The AMS provides detailed information about the chemical composition of the particulate matter, with the exception of refractory material such as metals and elemental carbon. In the AMS, the volatile and semi-volatile particulate species are ionized and fragmented before entering the mass spectrometer and the fragments of the original molecules are identified based on their mass-to-charge ratios. All of the ions measured for each fragment can be separated into their organic and inorganic components. The organic carbon content can be broken down into hydrocarbons (C_xH_y) and oxygenated hydrocarbons ($C_xH_yO_z$) and the inorganic content can be divided into sulfate, nitrate, and ammonium.

Figures 21 and 22 show the relative levels of inorganic matter, oxygenated hydrocarbons and hydrocarbons for the particulate matter for all nine fuels tested at 50% and 75% engine load, respectively. Figures 23 and 24 show the relative levels of nitrate, sulfate and ammonium within the inorganic particulate matter for the same conditions.

(See Figure 21 after last section of paper.)

(See Figure 22 after last section of paper.)

The results for the organic and inorganic content as shown in Figs. 21 and 22 are compared on the basis of signal intensity. It should be noted that these measurements are not normalized by engine load, so they cannot be compared directly with the results plotted in Figs. 19 and 20. However, the AMS data exhibit similar trends to those observed for the EC/OC analysis. At 50% load, the AMS data suggest that ULSD produced the lowest levels of OC (as signified by the sum of the oxygenated and non-oxygenated hydrocarbons), followed by the B20 methyl esters, with the exception of Algae 2 B20. For the B100 methyl esters at 50% load, Algae 2 B100 produced the lowest levels of OC while Algae 1 B100 produced the highest levels of OC. These results are consistent with the filter-based OC measurements. The relative levels of oxygenated hydrocarbons and inorganic compounds present in the particulate matter do not vary substantially between fuels. The AMS results at 75% load are similar to those at 50% load.

Figs. 23 and 24 show that all of the methyl esters produced higher levels of sulfates and ammonium in comparison to the ULSD at both loading conditions. Conversely, the relative levels of nitrates were approximately the same for the methyl esters in comparison to the ULSD, with the exception of the Canola B100, which exhibited high levels of nitrates for both loading conditions.

(See Figure 23 after last section of paper.)

(See Figure 24 after last section of paper.)

SUMMARY/CONCLUSIONS

The goal of this study was to characterize the performance and emissions from a diesel engine operating on FAME with fatty acid composition similar to that of the oil produced by several algal species currently under consideration for wide scale fuel production. Tests were performed on a John Deere 4024T, non-road diesel engine fitted with a unique, low-volume fuel injection system that enabled emissions tests to be conducted with very low volumes of specialty fuel sample. Tests were performed with ULSD, soy methyl ester, canola methyl ester and two methyl ester formulations with fatty acid composition similar to methyl esters produced from algal oil. The latter fuels were formulated based on the fatty acid composition of *Nannochloropsis Oculata* and *Isochrysis Galbana 3*, respectively. All of the methyl esters were tested in B20 blends with ULSD as well as B100. Exhaust gas measurements reported herein include brake specific mass emissions of NO_x, CO, THC, formaldehyde and acetaldehyde. Exhaust particulate measurements reported herein include total PM mass emissions, elemental carbon mass emissions, organic carbon mass emissions, PM size distribution and the chemical composition of the volatile and semi-volatile components of the PM. The latter measurements include relative levels of hydrocarbons, oxygenated hydrocarbons, nitrate, sulfate and ammonium content. In general, the performance and emissions characteristics of the algal methyl esters were similar to that of the methyl esters produced from the more traditional soy and canola feedstocks, with the exception of NO_x emissions which were lower for the algal methyl esters. In addition to the NO_x emissions results, the major conclusions of the study are summarized below.

• Brake Specific Fuel Consumption and Thermal Efficiency: Based on BSFC and thermal efficiency calculations, the performance of the engine when operating with algal methyl esters was similar to that of the soy and canola methyl esters. Specifically, all the B100 methyl esters resulted in increases in BSFC of 10 to 12 % with respect to ULSD. However, thermal efficiency calculations, which take into account the lower heating value of the methyl esters, show that the engine operated at a slightly higher overall efficiency on the methyl esters in comparison to ULSD.

• CO, THC: Emissions of CO and THC for the algal methyl esters were similar to that of the soy and canola methyl esters, which were similar to that reported in the literature.

• NO_x Emissions: Emissions of NO_x were shown to decrease for the algal methyl esters in comparison to the ULSD, in contrast to the soy and canola methyl esters which resulted in NO_x increases at the higher engine load. The decreased NO_x emissions from the algal methyl esters were accompanied by a decrease in premixed burn fraction.

• Aldehyde Emissions: Emissions of formaldehyde were found to increase slightly for the algal methyl ester formulations in comparison ULSD. In contrast, the soy and canola methyl esters resulted in decreases in formaldehyde emissions at both engine loading conditions. Acetaldehyde emissions decreased for all of the methyl esters in comparison to ULSD.

• PM Mass Emissions: PM mass emissions decreased substantially for all of the B100 methyl esters in comparison to ULSD at the high engine loading condition. At the lower engine loading condition, Algae 1 B100 had increased PM emissions in comparison to ULSD.

• EC/OC Particulate Mass Emissions: The PM from all of the methyl esters contained substantially higher quantities of

volatile organic carbon in comparison to ULSD, particularly at the lower engine loading condition. Algae 1 B100 had the highest ratio of OC:EC of all the fuels tested at both engine loading conditions.

• Particle Size Distributions: All of the B100 methyl esters resulted in a decrease in the mean mobility diameter. The PM size distribution from several of the methyl esters including Algae 1 B100 exhibited a nucleation mode peak centered between 10 and 20 nm.

• PM Chemical Composition: The relative quantity of oxygenated hydrocarbons present in the volatile organic PM was similar for all fuels tested. All of the methyl esters produced higher levels of sulfates and ammonium in comparison to the ULSD at both loading conditions.

This study represents a first attempt to examine the effect of long chain, highly unsaturated fatty acids found in algae oil on the combustion and emissions characteristics of transesterified methyl esters produced from these oils. The synthetic algal methyl ester formulations produced herein have fatty acid composition very close to methyl ester samples produce directly from algal oil. Therefore, the test results presented herein are not expected to deviate substantially from tests performed with transesterified algal oil. However, as higher quantities of algal oil become available the tests described herein should and will be repeated for direct comparison against these test results. It is also understood that, while these results suggest that the pollutant emissions from these fuels are similar to that measured from traditional methyl esters, initial test results suggest that other fuel properties such as oxidative/biological stability will be problematic. Future work should be done to accurately assess these and other fuel properties.

The conclusions stated above are relevant in the context of this particular engine class under several loading conditions. Future tests should also be conducted with modern on-road heavy duty diesel engines with common rail fuel injection systems and/or emissions control strategies that meet future EPA on-road emissions standards.

It also should be noted that the long chain, highly unsaturated fatty acids EPA and DHA currently have very high value as nutritional supplements. Therefore, it is expected that algal oil producers will make every effort to remove those constituents from algal oil prior to conversion of the oil into fuel. It is unclear at this time, however, as to what percentage of these constituents might remain in the oil after such a separation process. Moreover, the economic viability of such a separation process will evolve over time if large supplies of algal oil result in decreased value of EPA and DHA. Therefore, the results presented herein, along with future work on fuel characterization and emissions from fuels containing EPA and DHA will be useful to help guide future economic and environmental decisions related to fuels containing these constituents.

CONTACT INFORMATION

*Corresponding Author

Anthony J. Marchese
Associate Professor
Department of Mechanical Engineering
Colorado State University
1374 Campus Delivery
Fort Collins, CO 80523-1374
Phone: (970) 491-2328
Fax: (970) 491-3827
marchese@colostate.edu

ACKNOWLEDGMENTS

This work was supported by grants from the CSU Clean Energy Supercluster, the U.S. Small Business Administration and the National Science Foundation. The 4024T engine and financial support for its installation were provided by John Deere. The authors also wish to acknowledge the support of Teresa Alleman at the National Renewable Energy Laboratory in providing the fuel analysis.

REFERENCES

1. Shapouri, M.S., Duffield, J.A. and Wang, M. (2002). The Energy Balance of Corn Ethanol: An Update. United States Department of Agriculture, Agricultural Economic Report Number 814.

2. Graboski, M. S. (2002). Fossil Energy Use in the Manufacture of Corn Ethanol. Report Prepared for the National Corn Growers Association.

3. Van Gerpen, J. (2005). Biodiesel Processing and Production. *Fuel Processing Technology*, 86, 1097-1107

4. http://www.ricardo.com/media/pressreleases/pressrelease.aspx?page=148

5. Niven, R. K. (2005). Ethanol in gasoline: environmental impacts and sustainability review article. Sustainable Energy Reviews. Vol. 9, Issue 6, pp. 535-555

6. A Comprehensive Analysis of Biodiesel Impact on Exhaust Emissions. (2002). EPA420-P-02-001. Oct. 2002

7. Bennett, M., Volckens J., Stanglmaier R., McNichol A., Ellenson W., and Lewis C.. "Biodiesel Effects on Particulate Radiocarbon Emissions from a Diesel Engine." Aerosol Science, 2008: 667-678.

8. Jung, H. and Kittleson, D. B. (2006). Characteristics of SME Biodiesel-Fueled Diesel Particle Emissions and the Kinetics of Oxidation. Environmental Science and Technology, **40**, 4949-4955.

9. Krahl, J., Munack, A., Ruschel, Y., Schroder, O. et al., "Exhaust Gas Emissions and Mutagenic Effects of Diesel

Fuel, Biodiesel and Biodiesel Blends," SAE Technical Paper 2008-01-2508, 2008.

10. Sheehan, J., Dunahey, T., Benemann, J. and Roessler, P. (1998). A look back at the U.S. Department of Energy's Acquatic Species Program - Biodiesel from Algae. **NREL/ TP-580-24190**.

11. U.S. Department of Energy. National Algal Biofuels Technology Roadmap. DOE Biomass Program, 2009.

12. Kuronen, M., Mikkonen, S., Aakko, P., and Murtonen, T., "Hydrotreated Vegetable Oil as a Fuel for Heavy Duty Diesel Engines," SAE Technical Paper 2007-01-4031, 2007.

13. Knothe, G. (2005). Dependence of Biodiesel Fuel Properties on the Structure of Fatty Acid Alkyl Esters. Fuel Processing Technology, **86**, 1059-1070.

14. Graboski, M.S. and McCormick, R. L. (1998). Combustion of Fat and Vegetable Oil Derived Fuels in Diesel Engines. Prog. Energy Combust. Sci. **24**, pp. 125-164.

15. McCormick, R.L., Graboski, M.S., Alleman, T.L., Herring, A.M., Tyson, K.S. (2001). Impact of Biodiesel Source Material and Chemical Structure on Emissions of Criteria Pollutants from a Heavy-Duty Engine. Environmental Science and Technology. **35**, No. 9.

16. Schönborn, A., Ladommatos, N., Allan, R., Williams, J. et al., "Effect of Molecular Structure of Individual Fatty Acid Alcohol Esters (Biodiesel) on the Formation of NO_x and Particulate Matter in the Diesel Combustion Process," *SAE Int. J. Fuels Lubr.* **1**(1):849-872, 2008.

17. Han, M., Cho, K., Sluder, C.S., and Wagner, R.M., "Soybean and Coconut Biodiesel Fuel Effects on Combustion Characteristics in a Light-Duty Diesel Engine," SAE Technical Paper 2008-01-2501, 2008.

18. www.solixbiofuels.com

19. Fernandez-Feiriz, M., et al. (1989). "Biomass Production and Variation in the Biochemical Profile of Seven Species of Marine Microalgae." Aquaculture, 17-37.

20. Tonon, T., Harvey, D, Larson, T. R and Graham, I. A. (2002). Long chain polyunsaturated fatty acid production and portioning to triacylglycerols in four microalgae. Phytochemistry **16**: 15-24.

21. Spolare, P., Joannis-Cassan, C., Duran, E. and Isambert, A. (2006). Optimization of Nannochloropsis Oculata growth using the response surface method. *J. Chem. Technol. Biotechnol.* **81**; 1049-1056.

22. Bean-Amotz, A., Fishler, R. and Schneller, A. (1987). Chemical composition of dietary species of marine Unicellular algae and rotifiers with emphasis on fatty acids. Marine Biology **95**:31-36

23. Brown, M., Garland, C.D., Jeffrey, S. W., Jameson, I. D. and Le Roi, J. M. (1993). The gross amino acid compositions of batch and semi-continuous cultures of Isochrysis, Paavlova lutheri and Nannochloropsis Oculata. *Journal of Applied Phycology* **5**:285-296.

24. James, C. M., Al-Hinty, S., Salman, A. E. (1989). Growth and n-3 fatty acid and amino acid composition of microalgae under different temperature regimes. *Aquaculture* **77**:337-351.

25. Guckert, J. B. and Cooksey, K.e. (199). Triglyceride accumulation and fatty acid profile changes in Chlorella during high pH-induced cell cycle inhibition. *Journal of Phycology* **26**:72-79.

26. Kessler, E. (1980). Mass culture of Chlorella strains under conditions of high salinity, acidity and temperature. *Archive Hydrobiology* **60**:80-86.

27. Bennett, Maren. "Emissions from a Diesel Engine Operating with Soy-Based Biodiesel Fuel." Master's Thesis, Colorado State University, 2007.

28. Fisher, B. C. Characterization of Gaseous and Particulate Emissions from Algae-Based Methyl Ester Biodiesel. Masters Thesis, Colorado State University, 2009.

29. Lapuerta, M., Armas O., and Rodriguez-Fernandez J.. (2008). "Effect of Biodiesel Fuels on Diesel Engine Emissions." *Prog. Energy Combust. Sci.* 198-223.

30. McCormick, R.L., Williams A., Ireland J., Brimhall M., and Hayes R.R.. (2006). Effects of Biodiesel Blends on Vehicle Emissions. **NREL/MP-540-40554**.

31. Standards on Performance for Stationary Compression Ignition Internal Combustion Engines. 40 CFR Parts 60, 85 et al., Environmental Protection Agency, 2006.

32. Szybist, J.P. and Boehman, A.L., "Behavior of a Diesel Injection System with Biodiesel Fuel," SAE Technical Paper 2003-01-1039, 2003.

33. Patterson, J., Hassan, M.G., Clarke, A., Shama, G. et al., "Experimental Study of DI Diesel Engine Performance Using Three Different Biodiesel Fuels," SAE Technical Paper 2006-01-0234, 2006.

34. Szybist, J., Boehman, A., Taylor, J. and McCormick, R. *Fuel Processing Technology*, **86**, (2005) 1109.

35. Choi, C.Y., Bower, G.R., and Reitz, R.D., "Effects of Biodiesel Blended Fuels and Multiple Injections on D.I. Diesel Engines," SAE Technical Paper 970218, 1997.

36. Ban-Weiss, G.A., Chen, J.Y., Buchholz, B.A., and Dibble, R.W., *Fuel Processing Technology* **88**, (2007) 659-667.

37. Mueller, C.J., Boehman, A.L., and Martin, G.C., "An Experimental Investigation of the Origin of Increased NO_x Emissions When Fueling a Heavy-Duty Compression-Ignition Engine with Soy Biodiesel," *SAE Int. J. Fuels Lubr.* **2**(1):789-816, 2009.

38. Szybist, J., Song J., Alam M., and Boehman A.. (2007). "Biodiesel Combustion, Emissions and Emission Control." *Fuel Processing Technology* 679-691.

39. He, C., et al. (2009). "Comparison of Carbonyl Compounds Emissions from Diesel Engine Fueled with Biodiesel and Diesel." *Atmospheric Environment*, 3657-3661.

40. Di, Y., Cheung C., and Huang Z.. (2009) "Experimental Investigation on Regulated and Unregulated Emissions of a Diesel Engine Fueled with Ultra-low Sulfur Diesel Fuel Blended with Biodiesel from Waste Cooking Oil." *Science of the Total Environment.* 835-846.

41. Kittelson, D. (1998). "Engines and Nanoparticles: A Reveiw." *Journal of Aerosol Science*, 575-588.

42. Casati, R., Volker S., Vogt R., and Benter T. (2007) "Measurement of Nucleation and Soot Mode Particle Emission from a Diesel Passenger Car in Real World and Laboratory in Situ Diltuion." *Atmospheric Environment*, 2125-2135.

43. Kirchner, U., Scheer V., Vogt R., and Kagi R.. (2009) "TEM Study on Volatility and Potential Presence of Solid Cores in Nucleation Mode Particles from Diesel Powered Passenger Cars." *Aerosol Science*, 55-64.

44. Cheng, A.S., Buchholz, B.A., and Dibble, R.W., "Isotopic Tracing of Fuel Carbon in the Emissions of a Compression-Ignition Engine Fueled with Biodiesel Blends," SAE Technical Paper 2003-01-2282, 2003.

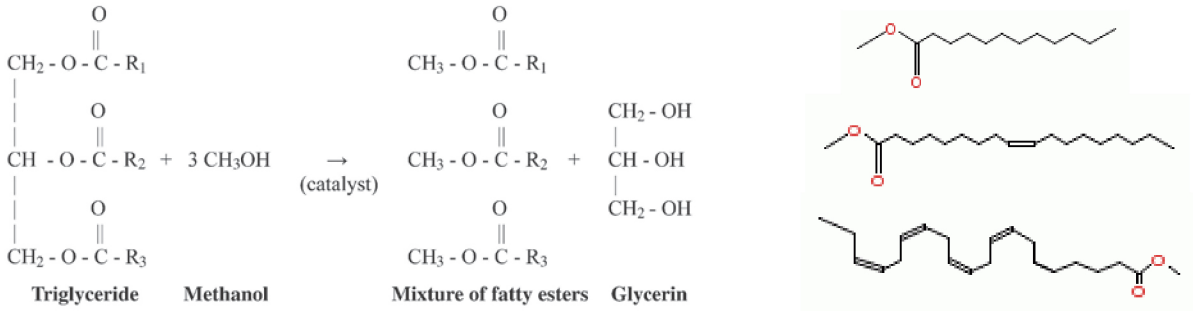

Figure 1. (a) Transesterification reaction converting triglycerides into FAME where R_1, R_2, and R_3 are hydrocarbon chains and (b) FAME constituents found in biodiesel: fully saturated methyl laurate (C12:0), mono-unsaturated methyl oleate (C18:1), and highly unsaturated eicosapentaeonic acid methyl ester (C20:5) in algae-derived FAME.

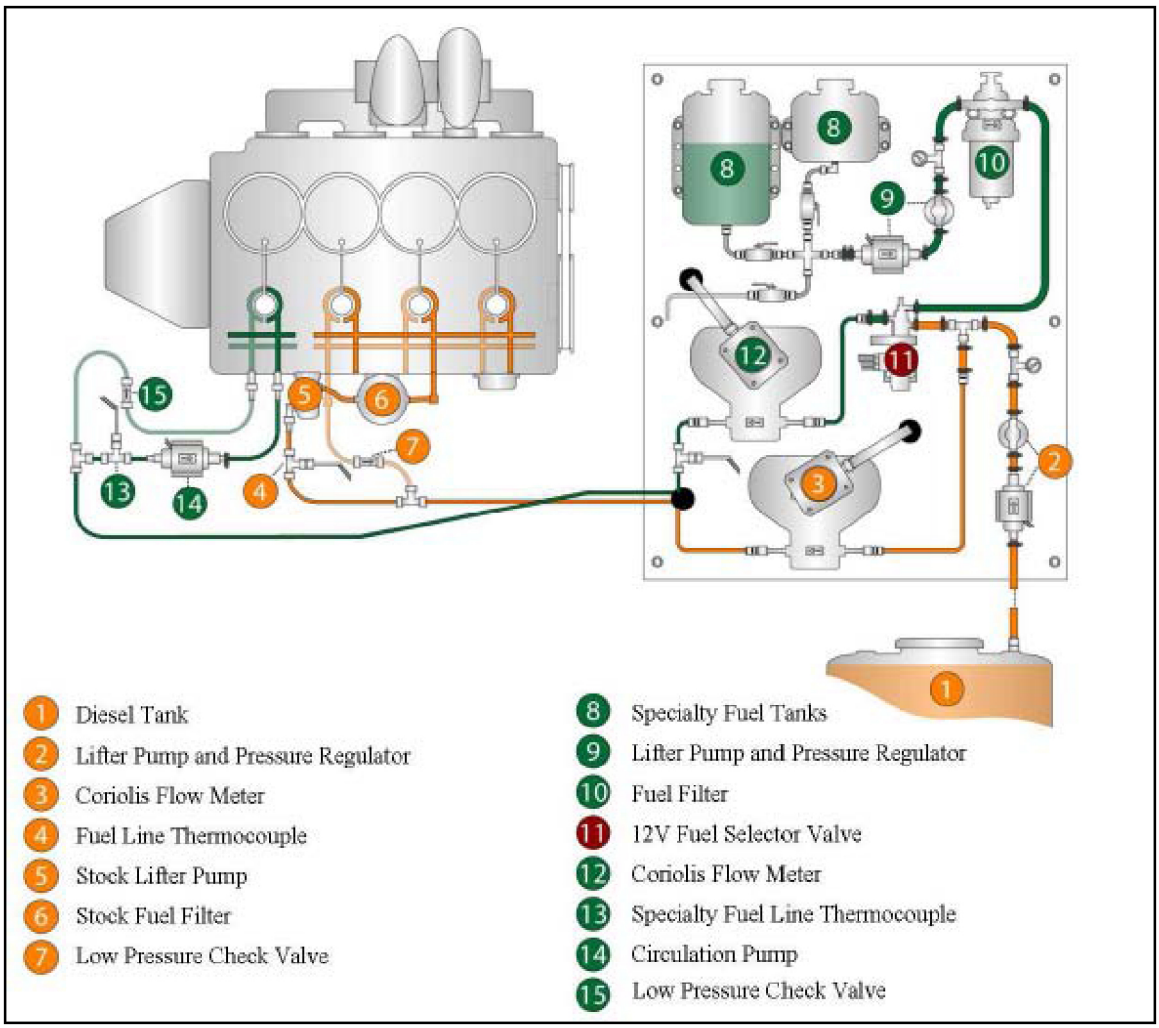

Figure 2. Schematic diagram of redesigned fuel injection system for the 4024T engine

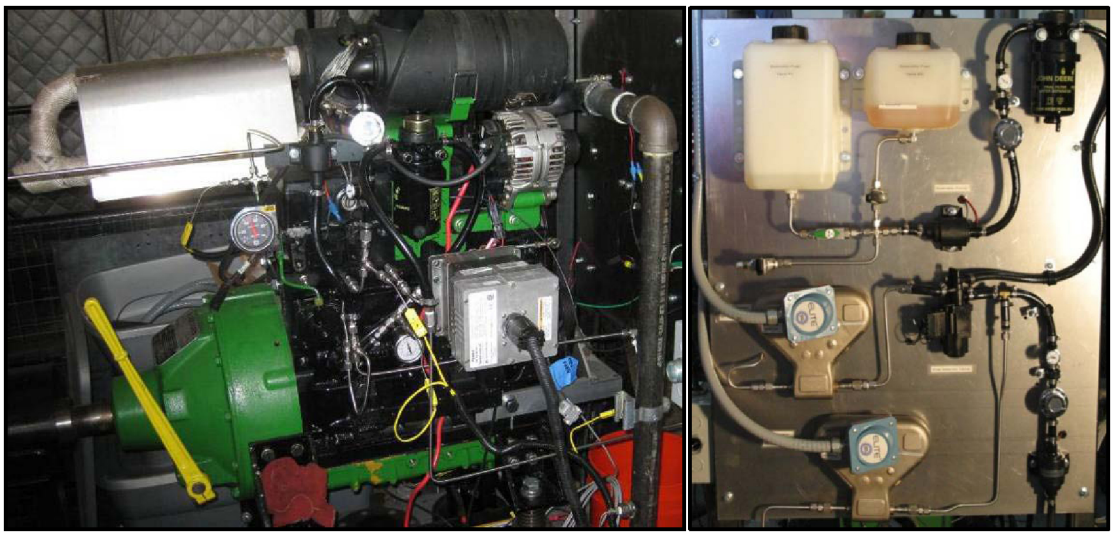

Figure 3. Completed fuel injection system and instrumentation panel.

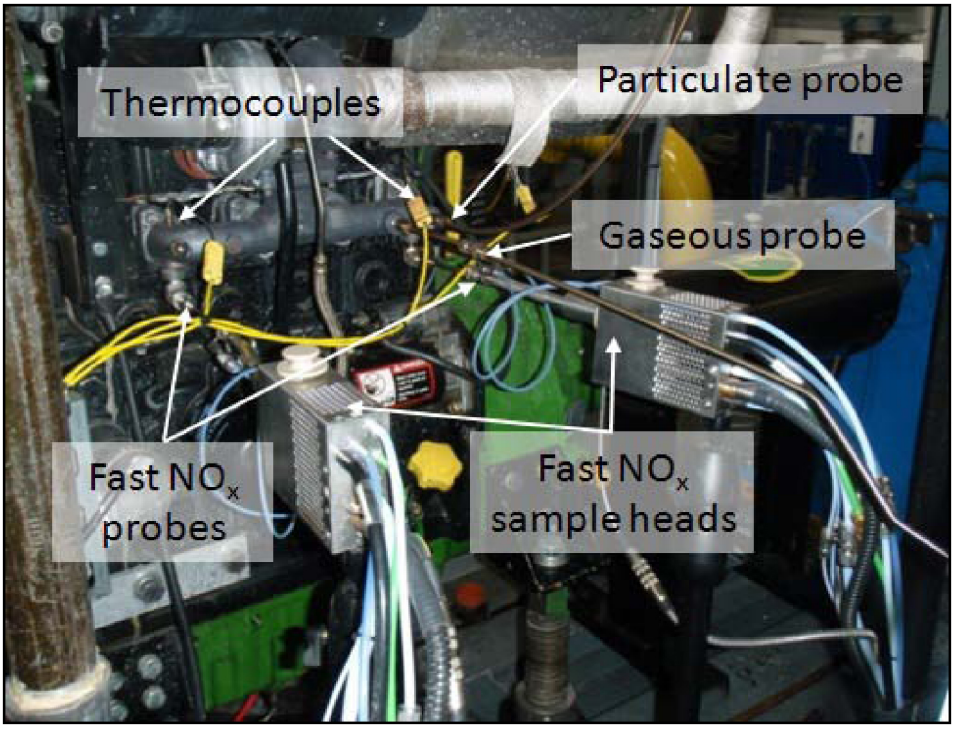

Figure 4. Photograph of all the probes installed on the exhaust manifold. Cylinder 1 is located on the left; cylinder 4 is on the right.

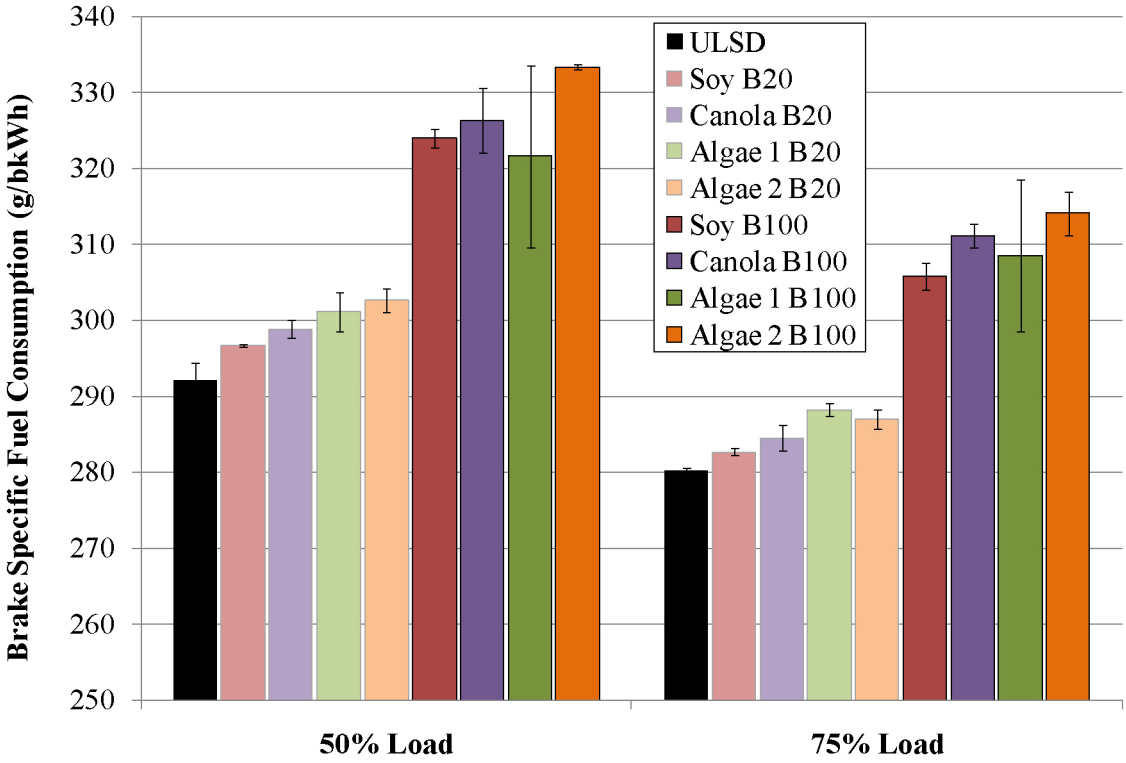

Figure 5. Brake specific fuel consumption (g/bkWh) for John Deere 4024T engine for 9 different fuel types at rated speed (2400 RPM) and 50% and 75% load. The error bars represent the range of the two tests conducted for each fuel/engine load condition.

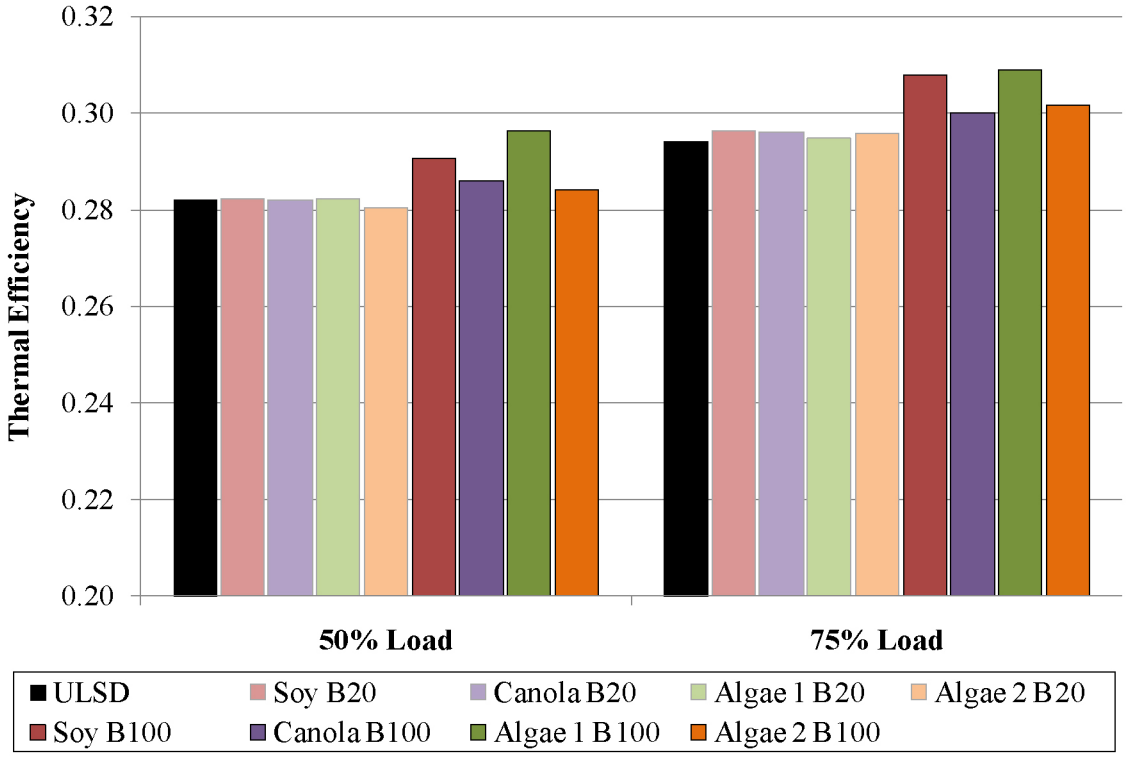

Figure 6. Average thermal efficiency for all nine fuels at both loads.

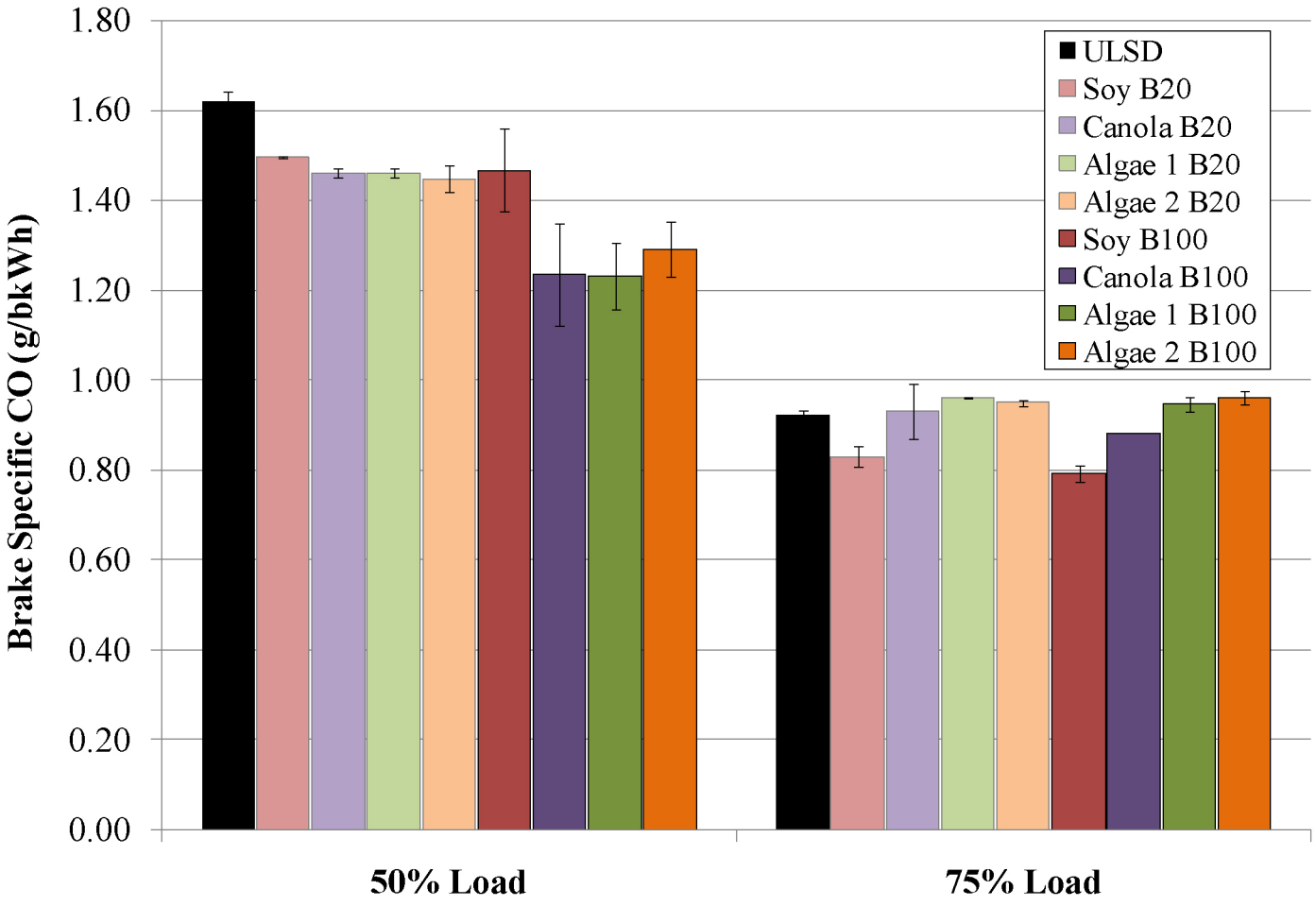

Figure 7. Brake specific carbon monoxide emissions (g/bkWh) for John Deere 4024T engine for 9 different fuel types at rated speed (2400 RPM) and 50% and 75% load.

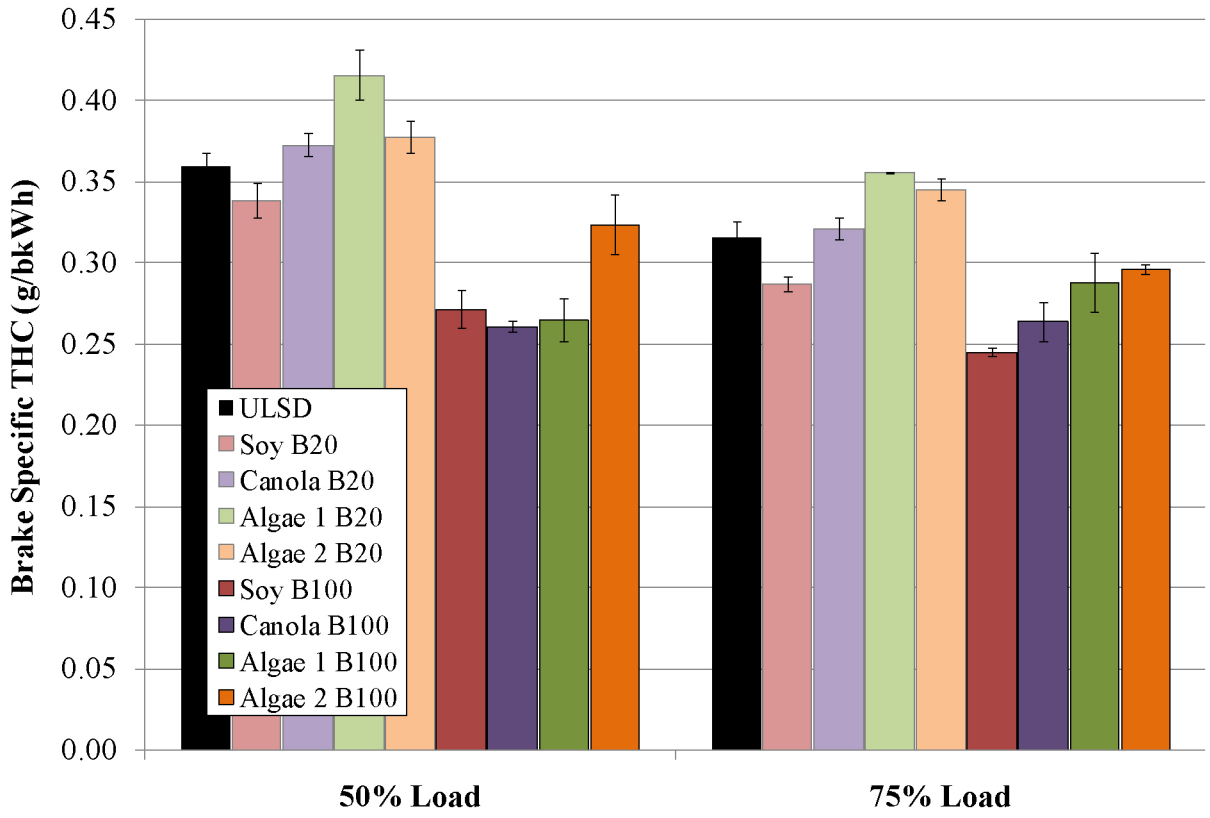

Figure 8. Brake specific total hydrocarbon emissions (g/bkWh) for John Deere 4024T engine for 9 different fuel types at rated speed (2400 RPM) and 50% and 75% load.

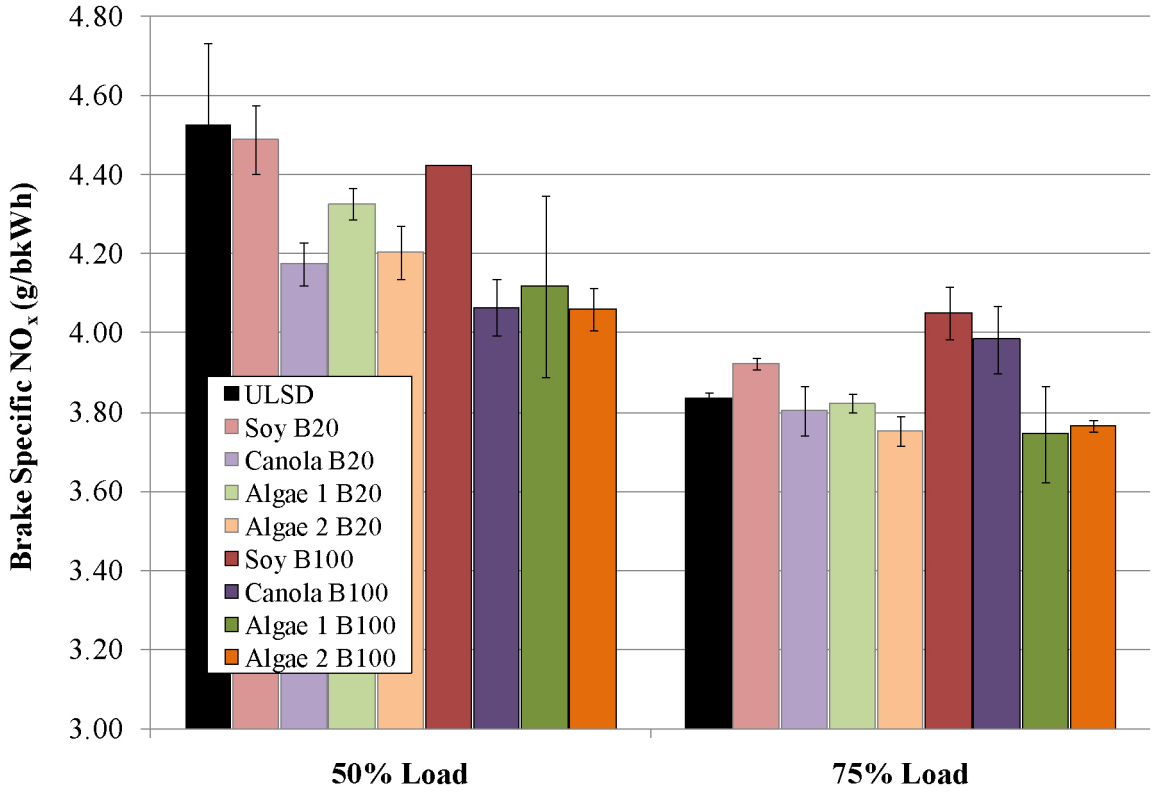

Figure 9. Brake specific NO_x emissions (g/bkWh) for John Deere 4024T engine for 9 different fuel types at rated speed (2400 RPM) and 50% and 75% load.

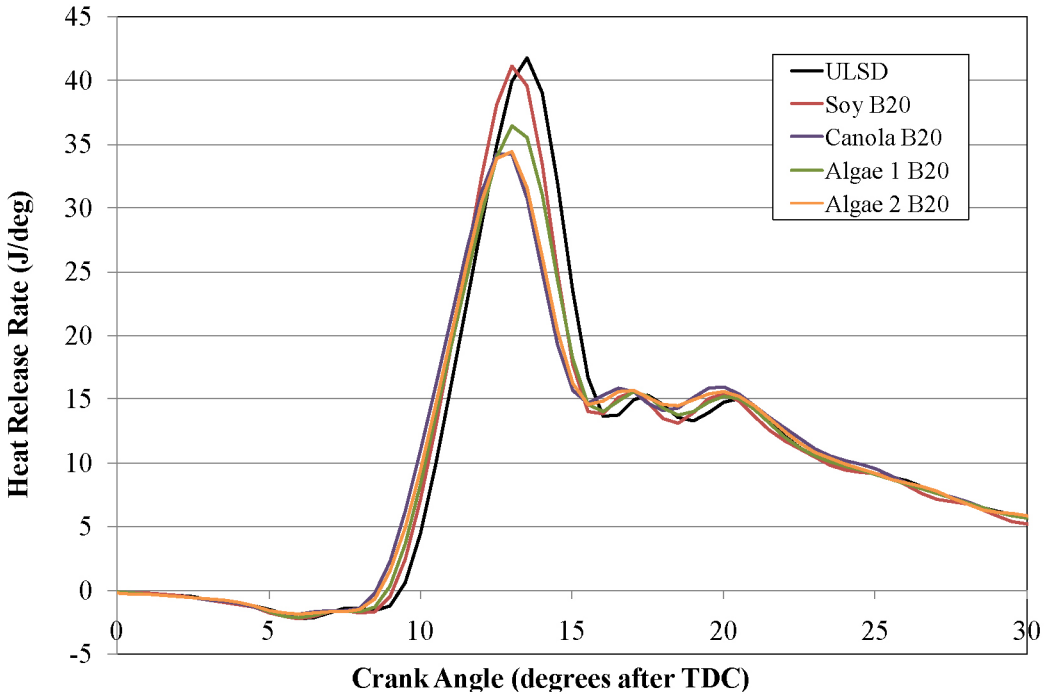

Figure 10. Apparent Rate of Heat Release (J/deg) from John Deere 4024T engine for B20 Blends at 50% load.

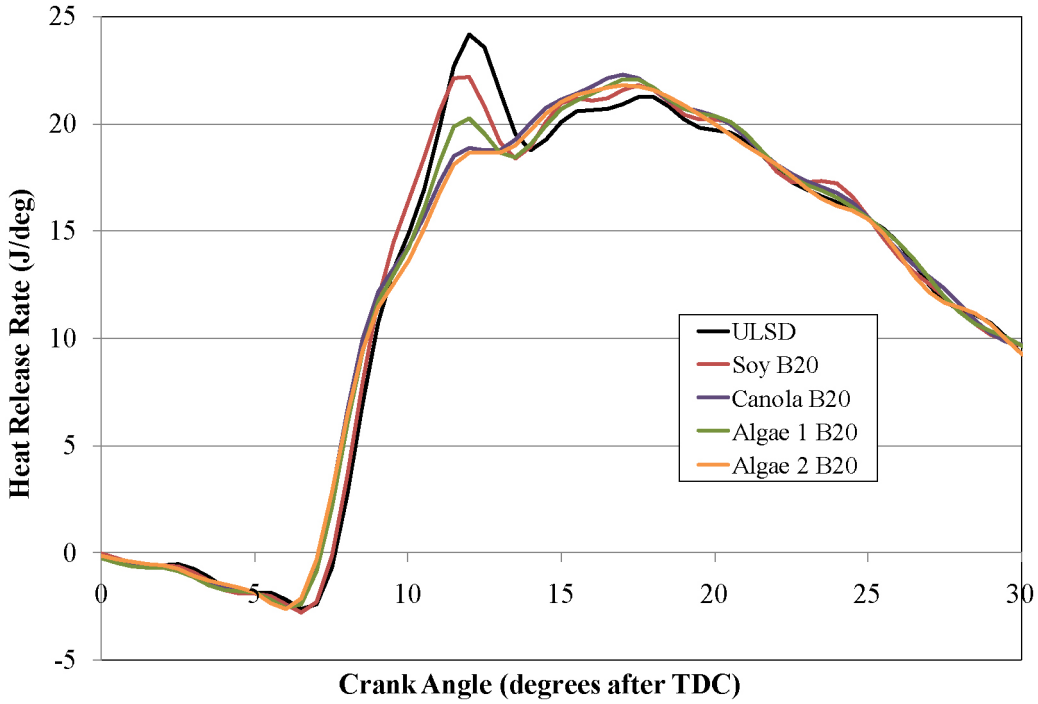

Figure 11. Apparent Rate of Heat Release (J/deg) from John Deere 4024T engine for B20 Blends at 75% load.

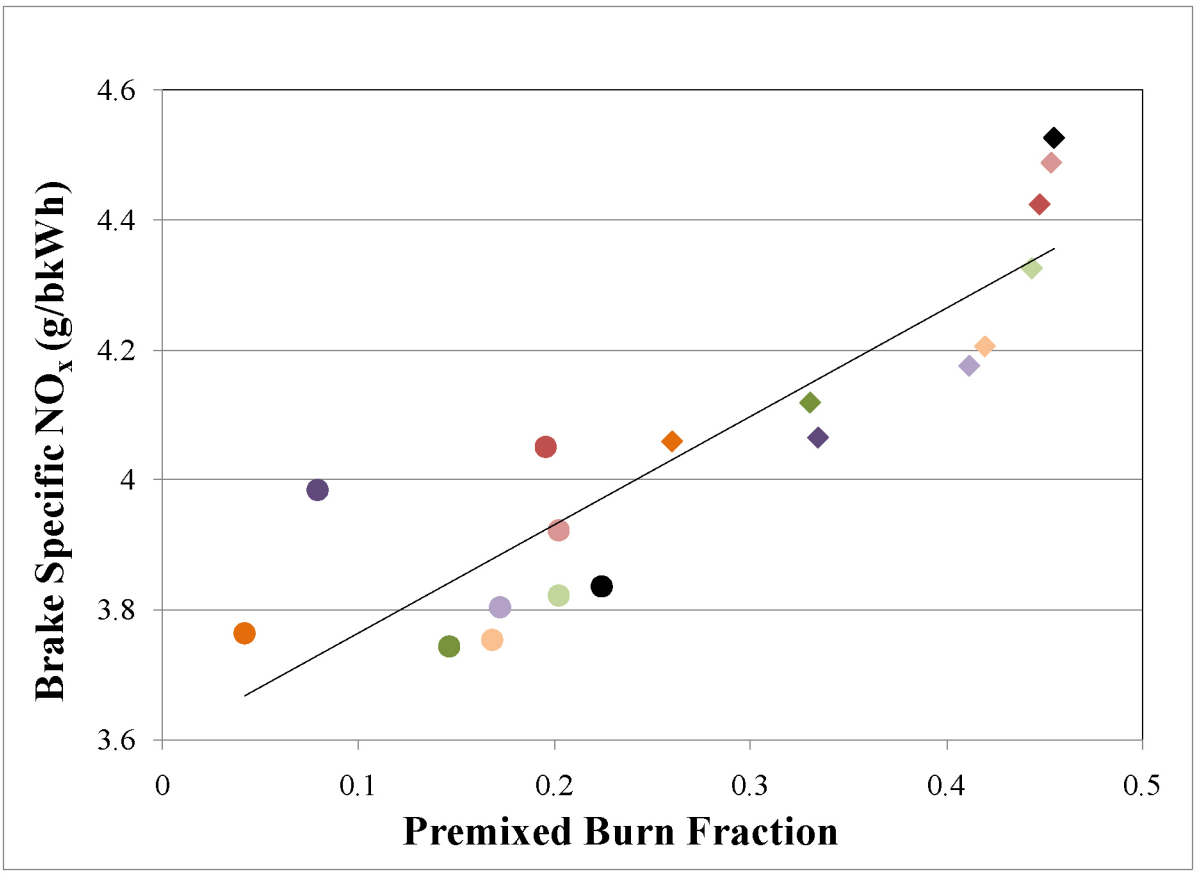

Figure 12. Relationship between brake specific NO_x emissions and premixed burn fraction. The data points are colored to show fuel type. Diamond-shaped data points correspond to 50% load; round data points denote 75% load.

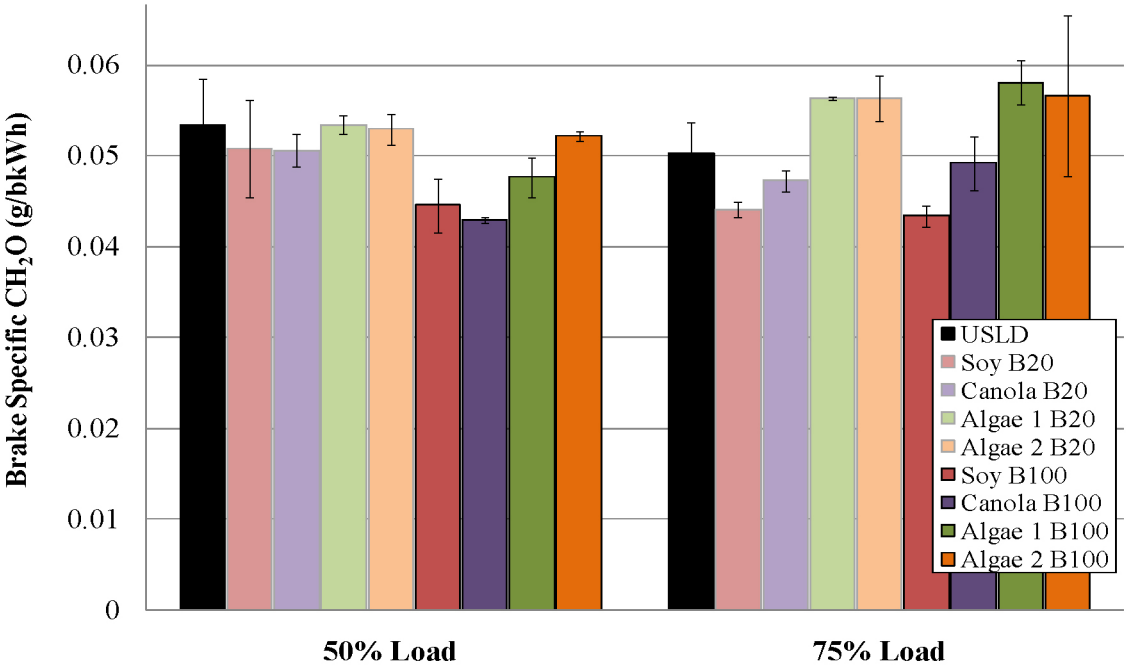

Figure 13. Brake specific formaldehyde emissions (g/bkWh) for John Deere 4024T engine for 9 different fuel types at rated speed (2400 RPM) and 50% and 75% load. The error bars represent the range of the two runs for each data point.

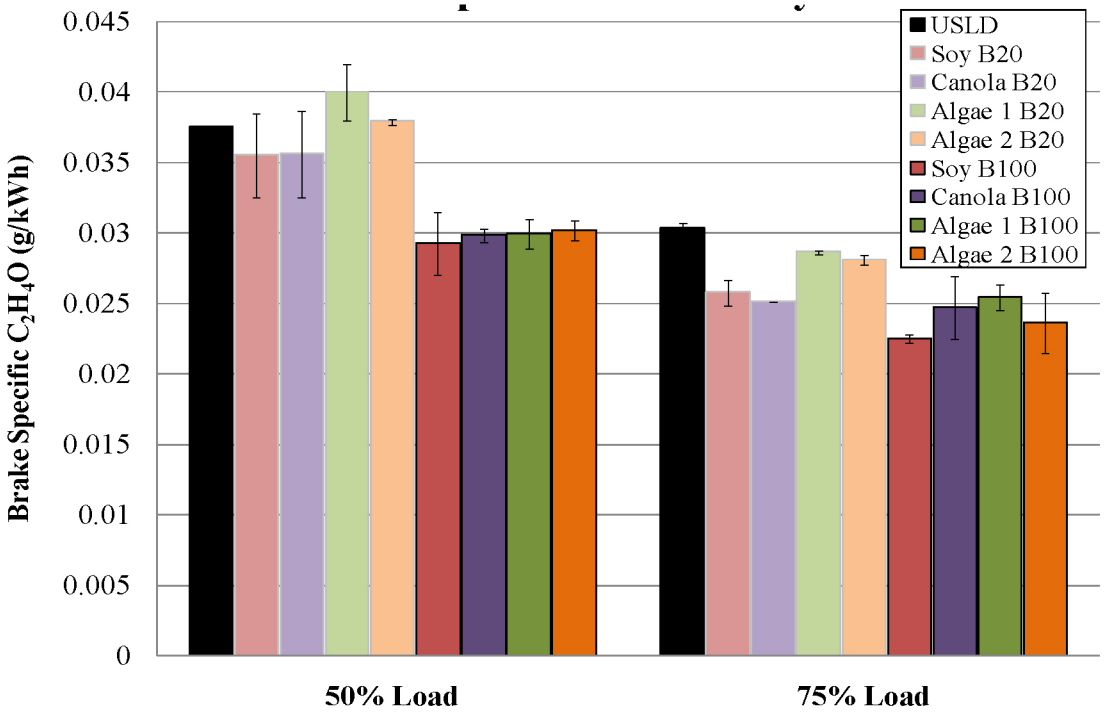

Figure 14. Brake specific acetaldehyde emissions (g/kW-hr) for John Deere 4024T engine for 9 different fuel types at rated speed (2400 RPM) and 50% and 75% load.

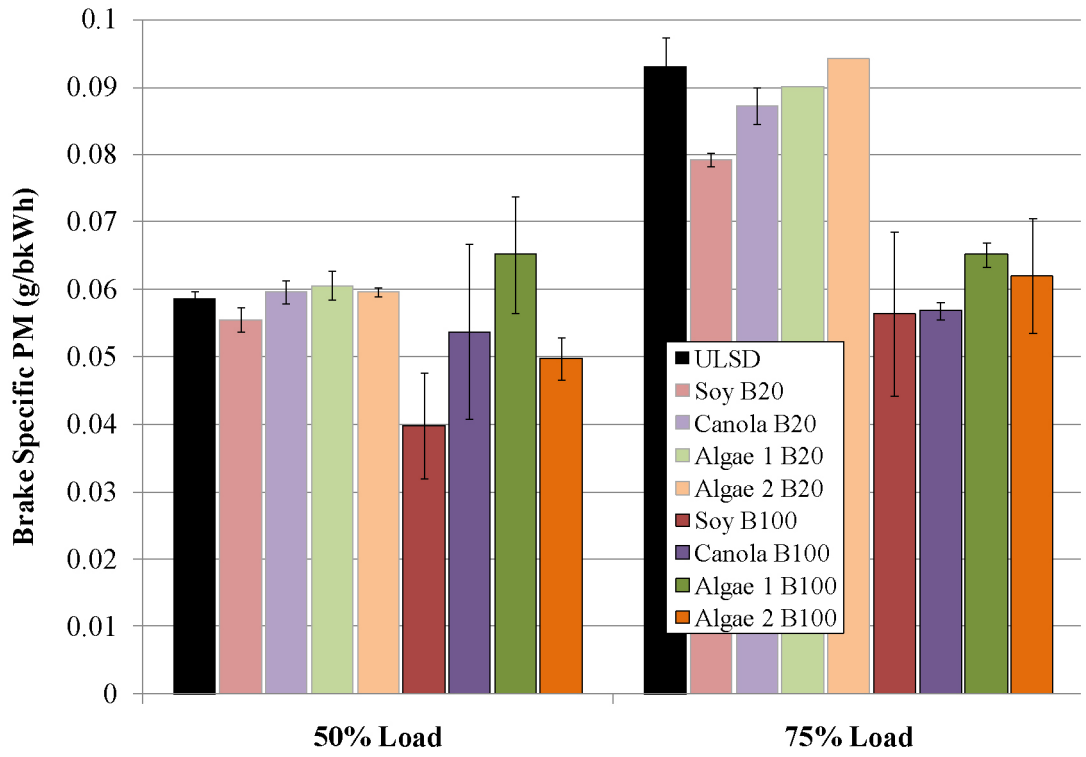

Figure 15. Brake specific total particulate matter mass emissions (g/kWh) for John Deere 4024T engine for 9 different fuel types at rated speed (2400 RPM) and 50% and 75% load. The error bars represent the range of the two runs for each data point.

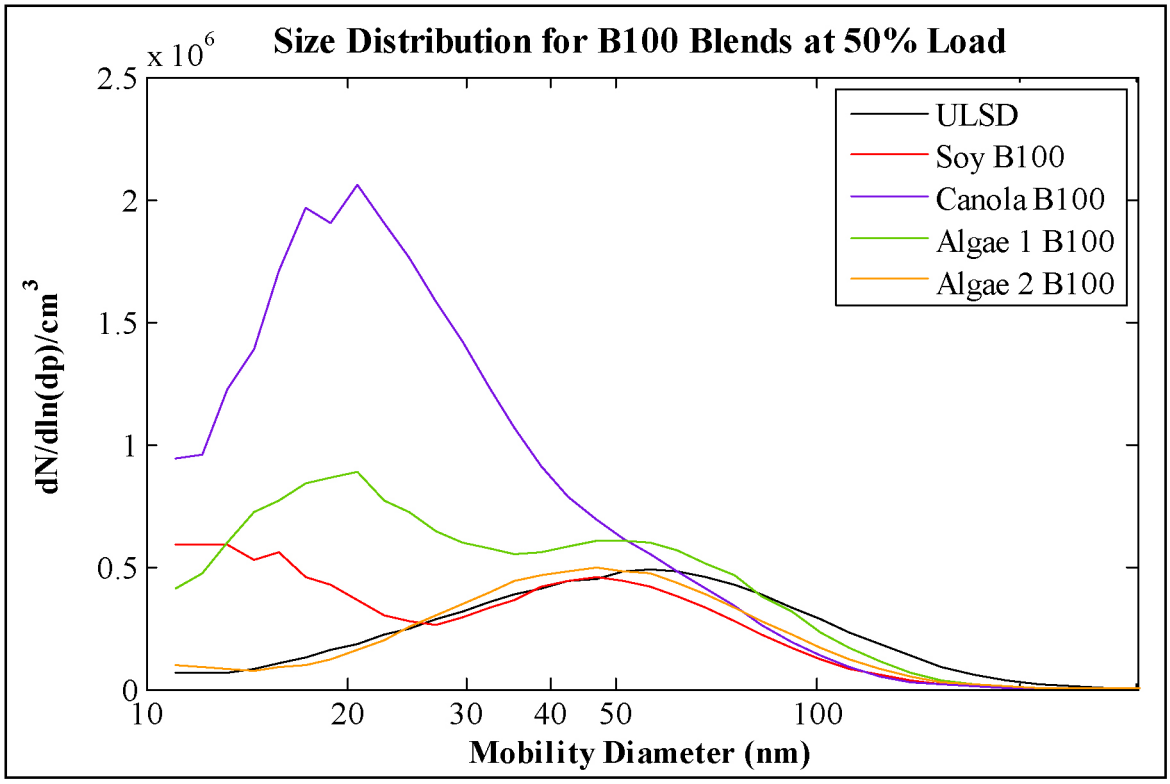

Figure 16. Particulate matter size distribution for B100 blends at rated speed, 50% load.

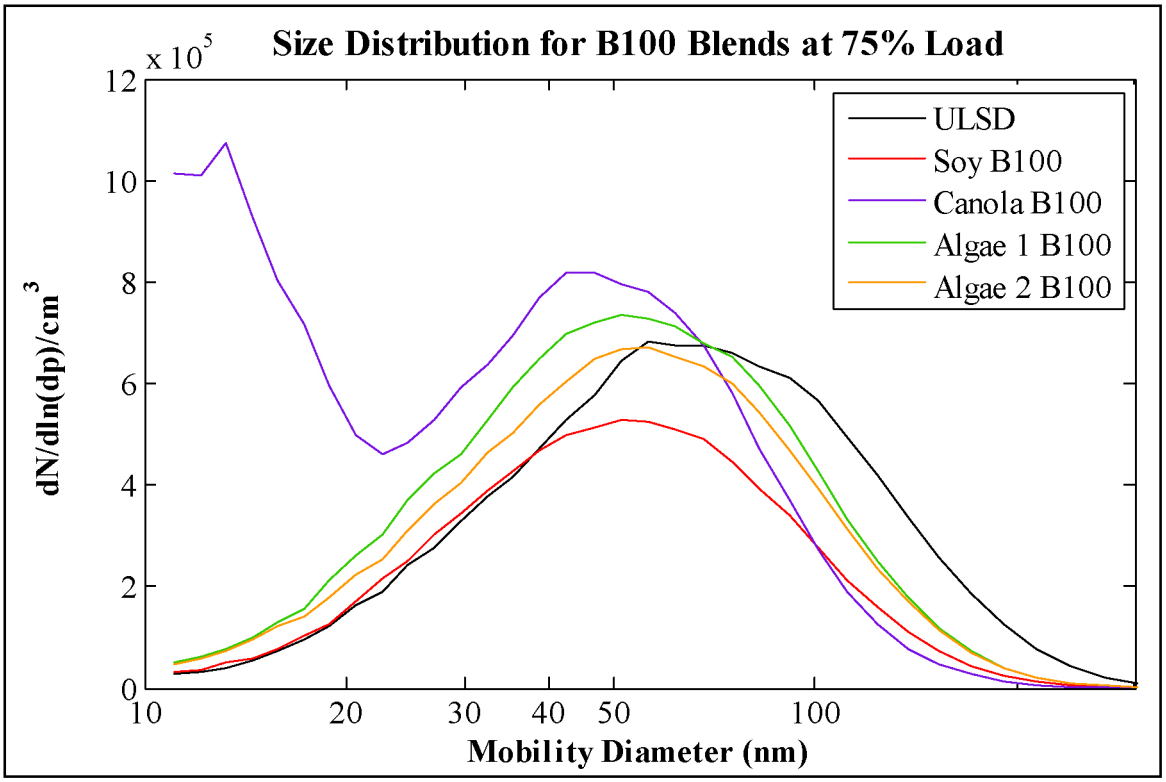

Figure 17. Particulate matter size distribution for B100 blends at rated speed, 75% load.

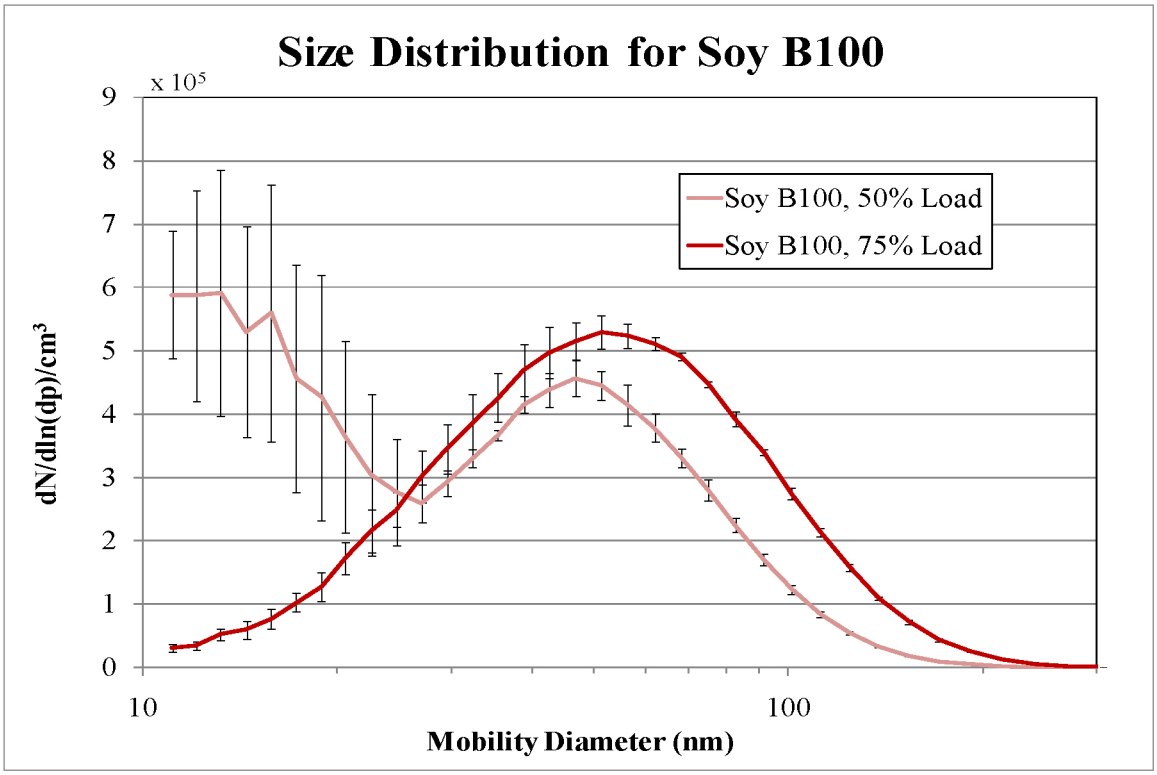

Figure 18. Particulate matter size distribution for Soy B100 at 50% and 75% load with standard deviation error bars shown.

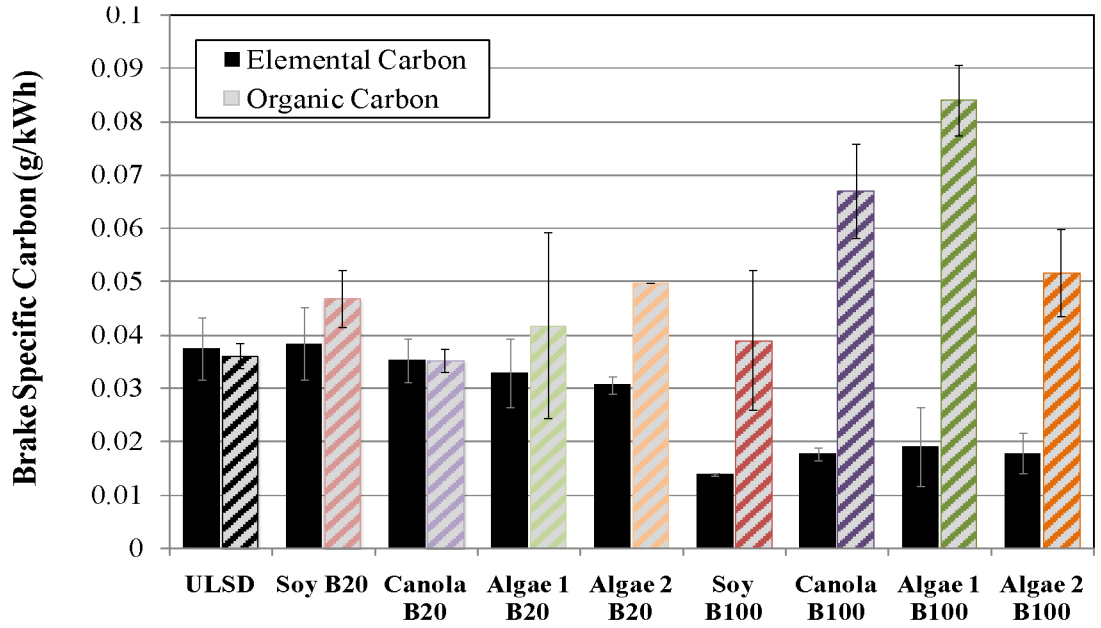

Figure 19. Elemental and Organic Carbon for 9 different fuel types at rated speed and 50% load. The error bars represent the range of the two tests conducted at each operating condition.

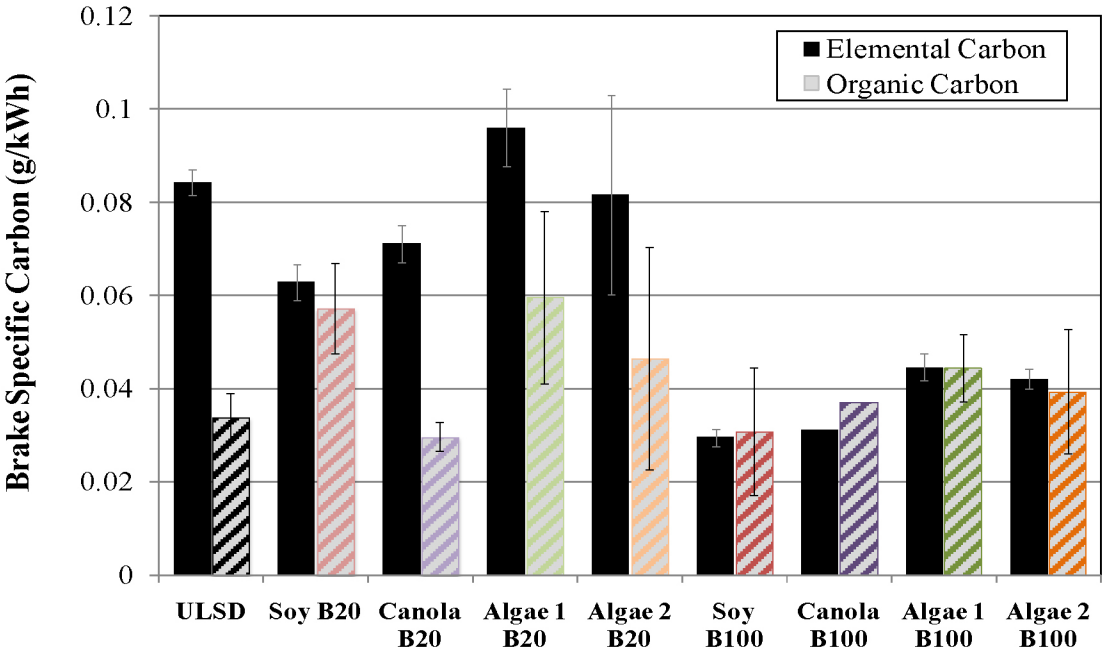

Figure 20. Elemental and Organic Carbon for 9 different fuel types at rated speed and 75% load. The error bars represent the range of the two tests conducted at each operating condition.

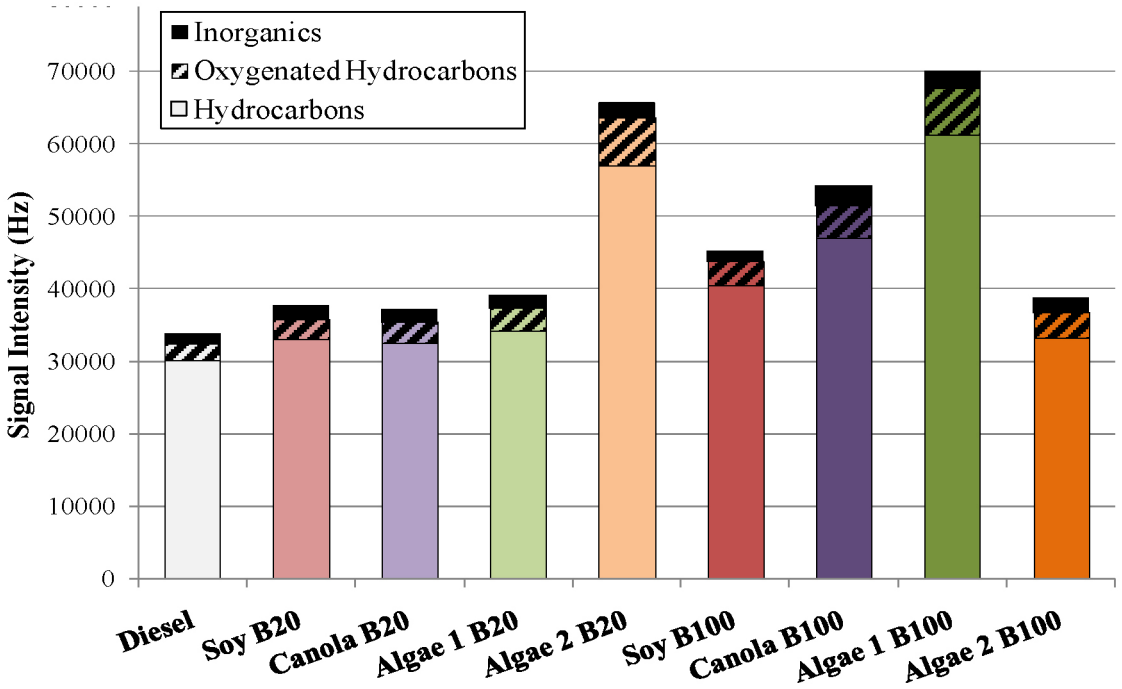

Figure 21. Relative levels of inorganic matter, oxygenated hydrocarbons and hydrocarbons for the particulate matter from all nine fuels tested at 50% engine load.

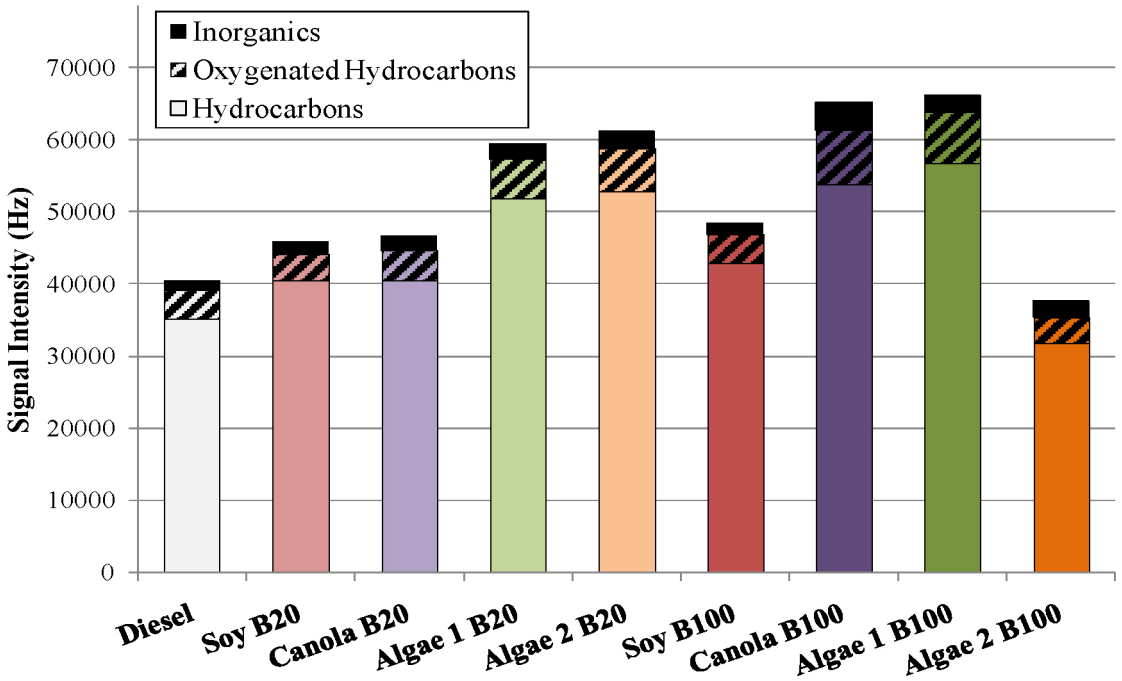

Figure 22. Relative levels of inorganic matter, oxygenated hydrocarbons and hydrocarbons for the particulate matter from all nine fuels tested at 75% engine load.

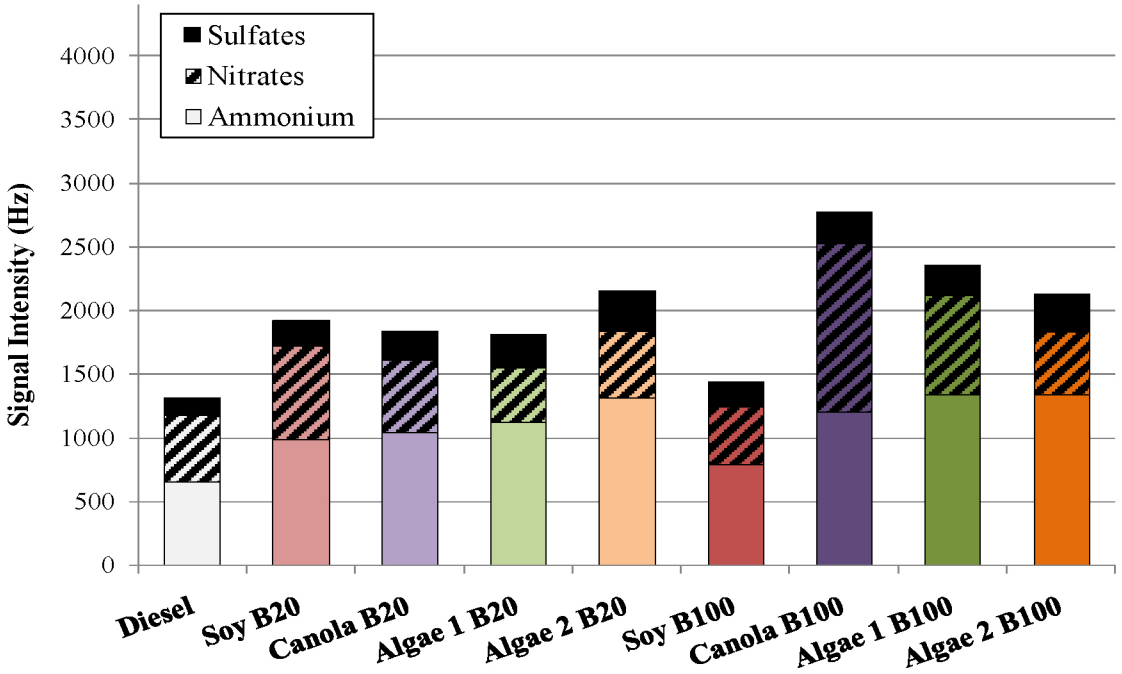

Figure 23. Relative levels of nitrate, sulfate and ammonium within the inorganic particulate matter from all nine fuels at 50% engine load.

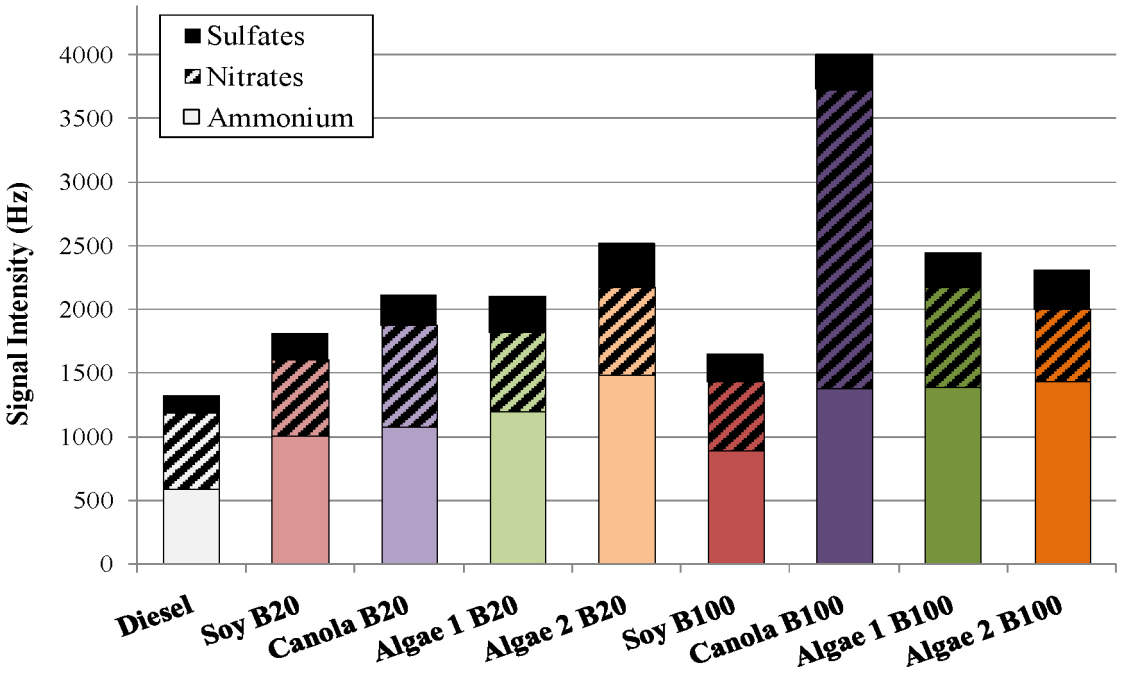

Figure 24. Relative levels of nitrate, sulfate and ammonium within the inorganic particulate matter from all nine fuels at 75 % engine load.

Table 1. Approximate weight percent of fatty acids in various vegetable and algal oil feedstocks [15,19, present work]. The nomenclature Cx:y denotes the length of the hydrocarbon chain (x) and the number of double bonds in the hydrocarbon chain (y) of the fatty acid.

Feedstock	C8:0	C10:0	C12:0	C14:0	C16:0	C16:1	C18:0	C18:1	C18:2	C18:3	C20:0	C20:4	C20:5	C22:6
Soy					10		4	24	54	8				
Canola					5		2	64	20	8				
Coconut	9	6	49	17	8		2	5	2					
Palm				1	42		5	41	10					
Jatropha					11		17	13	47		5			
Nannoch. Oculata				4	29	24	9	4	1	1		5	22	
Iso. Galbana				13	36	32	1	4	4				7	3

Table 2. Fatty acid composition (per cent volume) of composite algal oil formulations in comparison to that of Nannochloropsis Oculata and Isochrysis Galbana 3.

	Nanochl. Occul.	Composite	Iso. Galbana	Composite
Cx:0	33.78	32.39	51.40	47.37
Cx:1	32.84	34.96	35.69	36.05
Cx:2	3.55	3.17	3.64	3.84
Cx:3	2.32	0.78	0.00	0.33
Cx:4+	22.39	23.55	9.25	10.09

Table 3. Selected fuel properties as measured in this study for ULSD and the B100 methyl ester blends.

	ULSD	Soy	Canola	Algae 1	Algae 2
Density (kg/m^3)	840.5	885.6	882.5	889.2	879.7
Bulk Modulus (GPa)	1.584	1.777	1.767	1.786	1.741
LHV (MJ/kg)	42.78	37.27	37.32	37.12	37.13
Cloud Point (°C)	-12.1	0.6	-3.2	6.4	12.2
Sulfur (ppm)	6.8	2.7	1.9	14	7
Free Glycerides (wt%)	-	.029	.005	.002	.002
Total Glycerides (wt%)	-	.202	.415	.071	.037
Mono Glycerides	-	.58	.811	.18	.09
DiGlycerides	-	.114	.613	.076	.038
TriGlycerides	-	.048	.048	.109	.061